CATÓLICA
ESCOLA SUPERIOR DE BIOTECNOLOGIA

PORTO

INTELLIGENT COMPUTATIONAL SYSTEM FOR COLONY-FORMING-UNIT ENUMERATION AND DIFFERENTIATION

by
Jorge Miguel Borges Caeiro Luís

February 2021

CATÓLICA
ESCOLA SUPERIOR DE BIOTECNOLOGIA

PORTO

INTELLIGENT COMPUTATIONAL SYSTEM FOR COLONY-FORMING-UNIT ENUMERATION AND DIFFERENTIATION

Thesis presented to Escola Superior de Biotecnologia of the Universidade Católica Portuguesa to fulfill the requirements of Master of Science degree in Biomedical Engineering

by
Jorge Miguel Borges Caeiro Luís

Supervisor: Prof.ª Doutora Freni Kekhasharú Tavaria
Escola Superior de Biotecnologia, Universidade Católica Portuguesa

Co-Supervisor: Prof. Doutor Pedro Miguel de Luís Rodrigues
Escola Superior de Biotecnologia, Universidade Católica Portuguesa

February 2021

Abstract

Accurate quantitative analysis of microorganisms is recognized as an essential tool for gauging safety and quality in a wide range of fields. The enumeration processes of viable microorganisms via traditional culturing techniques are methodically convenient and cost-effective, conferring high applicability worldwide. However, manual counting can be time-consuming, laborious and imprecise. Furthermore, particular pathologies require an urgent and accurate response for the therapy to be effective. To reduce time limitations and perhaps discrepancies, this work introduces an intelligent image processing software capable of automatically quantifying the number of Colony Forming Units (CFUs) in Petri-plates. This rapid enumeration enables the technician to provide an expeditious assessment of the microbial load. Moreover, an auxiliary system is able to differentiate among colony images of *Echerichia coli*, *Pseudomonas aeruginosa* and *Staphylococcus aureus* via Machine Learning, based on a Convolutional Neural Network in a process of cross-validation. For testing and validation of the system, the three bacterial groups were cultured, and a significant labeled database was created, exercising suited microbiological laboratory methodologies and subsequent image acquisition. The system demonstrated acceptable accuracy measures; the mean values of precision, recall and F-measure were 95%, 95% and 0.95, for *E. coli*, 91%, 91% and 0.90 for *P. aeruginosa*, and 84%, 86% and 0.85 for *S. aureus*. The adopted deep learning approach accomplished satisfactory results, manifesting 90.31% of accuracy. Ultimately, evidence related to the time-saving potential of the system was achieved; the time spent on the quantification of plates with a high number of colonies might be reduced to a half and occasionally to a third.

Keywords: Colony Forming Units, Petri-plates, image processing, enumeration, Convolutional Neural Network.

Resumo

A análise quantitativa de microrganismos é uma ferramenta essencial na aferição da segurança e qualidade numa ampla variedade de áreas. O processo de enumeração de microrganismos viáveis através das técnicas de cultura tradicionais é económica e metodologicamente adequado, conferindo-lhe alta aplicabilidade a nível mundial. Contudo, a contagem manual pode ser morosa, laboriosa e imprecisa. Em adição, certas patologias requerem uma urgente e precisa resposta de modo a que a terapia seja eficaz. De forma a reduzir limitações e discrepâncias, este trabalho apresenta um software inteligente de processamento de imagem capaz de quantificar automaticamente o número de Unidades Formadoras de Colónias (UFCs) em placas de Petri. Esta rápida enumeração, possibilita ao técnico uma expedita avaliação da carga microbiana. Adicionalmente, um sistema auxiliar tem a capacidade de diferenciar imagens de colónias de *Echerichia coli*, *Pseudomonas aeruginosa* e *Staphylococcus aureus* recorrendo a Machine Learning, através de uma Rede Neuronal Convolucional num processo de validação cruzada. Para testar e validar o sistema, os três grupos bacterianos foram cultivados e uma significativa base de dados foi criada, recorrendo às adequadas metodologias microbiológicas laboratoriais e subsequente aquisição de imagens. O sistema demonstrou medidas de precisão aceitáveis; os valores médios de precisão, recall e F-measure, foram 95%, 95% e 0.95, para *E. coli*, 91%, 91% e 0.90 para *P. aeruginosa*, e 84%, 86% e 0.85 para *S. aureus*. A abordagem deep learning obteve resultados satisfatórios, manifestando 90.31% de precisão. O sistema revelou potencial em economizar tempo; a duração de tarefas afetas à quantificação de placas com elevado número de colónias poderá ser reduzida para metade e ocasionalmente para um terço.

Palavras-chave: Unidades Formadoras de Colónias, placas de Petri, processamento de imagem, enumeração, Rede Neuronal Convolucional.

Aknowlegements

First and foremost, I would like to sincerely thank to my Supervisors, Professor Freni Tavaria and Professor Pedro Rodrigues. I thank you both for your excellent guidance and support at all times, as well as the constantly positive and motivating athmosphere.

I would also like to thank Mariana, my colleague at the Microbiology Laboratory, and to past and present colleagues at Escola Superior de Biotecnologia.

Finally, I would like to thank my family – Mother, Father and Sister – for their encouragement, patience and love.

Jorge Caeiro Luís

"Prediction by analogy – creativity – is so pervasive we normally don't notice it"

Jeff Hawkins

Outline

List of Figures

List of Tables

Abbreviations and Symbols

BHI	Brain Hearth Broth
CO_2	Carbon Dioxide
CB	Catchment basin
°C	Celsius degrees
CINATE	Center for Innovation and Technological Support
cm	Centimeter
CPU	Central Processing Unit
CCD	Charge-coupled Device
CFU	Colony Forming Unit
CNN	Convolutional Neural Network
CS	Cross section
DNA	Deoxyribonucleic Acid
E. coli	*Echerichia coli*
EM	Electromagnetic Spectrum
ESB	Escola Superior de Biotecnologia
EN	European Standards
EMAX	Extended Maxima
EMIN	Extended Minima
FC	Fully Connected
GHz	Giga Hertz
g	Gram
GPU	Graphical Processing Unit
GUI	Graphical User Interface
HE	Hektoen Enteric Agar
HMAX	H-Maxima Transformation
HMIN	H-Minima Transformation
IZ	Influence Zone
ISO	International Organization for Standardization
LDPE	Low-density Polyethylene

MRI	Magnetic Resonance Imaging
μL	Microliter
mL	Milliliter
mm	Millimeter
MPN	Most Probable Number
MLR	Multilinear Regression
PDAF	Phase-Detection Autofocus
PCA	Principal Component Analysis
P. aeruginosa	*Pseudomonas aeruginosa*
RMM	Rapid Microbiological Methods
ROC	Receiver Operating Curve
ReLU	Rectified Linear Unit
RBC	Red blood cell
RMAX	Regional Maxima
RMIN	Regional Minima
ROI	Return of Investment
SKIZ	Skeleton by Influence Zone
S. aureus	Staphylococcus aureus
SGD	Stochastic Gradient Descent
SE	Structuring element
SVM	Support Vector Machine
TNTC	Too numerous to count
TSA	Tryptic Soy Agar
VNBC	Viable but nonculturable

CHAPTER 1

Introduction

1.1 Rationale

The assessment of bacterial growth is an essential procedure in several studies on microorganisms. Evaluation of food and drug safety, control of environmental quality and the selection of antibiotics, are fields that rely on the measurement of microorganism survival and proliferation rates. Due to its importance, this evaluation has been and will continue to be widely employed worldwide on a daily basis. Therefore, the improvement of the available techniques and practices is appreciated. The above-mentioned processes often require the counting of bacteria in a unit volume of bacterial broth and there are several methods available that can achieve it in a direct or indirect way; cytometry and microscopic counts as direct measures, and turbidity, metabolic activity, membrane filtration, dry weight and the agar plate method as indirect measures. Of these methods, the agar plate method is the most cost-effective, easily-accessed but yet accurate method. When performing this method, the viable number of bacteria can be obtained by counting the number of colonies on the plate. However, the manual counting of colonies is laborious, time-consuming and error-prone. In addition, particular pathologies require a fast response in order to reach an effective therapy. Image processing techniques are thus seen as a potential option for performing the counting tasks. With the development of this work, some of these limitations are expected to be reduced or overcomed.

1.2 Related Works

According to the state-of-the-art related with this subject, several image processing software programs have been developed. In [1] was created and proposed a low-cost, high-throughput process consisting of a colony counting system and a consumer-grade digital camera. The software, called

NICE, can count bacterial colonies as part of a high-throughput multiplexed opsonophagocytic killing assay used to characterize pneumococcal vaccine efficacy. It reads standard image formats, and therefore may be used in conjunction with other imaging system. *Clono-Counter*, developed in [2], is a colony counting software through the use of three parameters, i.e. maximum size of the colony, gray levels and gray level distribution. Despite provided guidelines, the users need to have some experience to find the correct parameters. A fully-automated colony counter for bacterial colony enumeration was proposed in [3] with considerable accuracy to detect colonies cultivated in colored media but has limitations with those with transparent media. Two years later, the same authors developed a method to allow enumerations in a wider range of media with a reasonable performance on both colored and translucent media [3]. In [4] a CCD camera was used to capture images of colonies and images were treated as perfect circles, removing the boundary and consequently the linked colonies, underestimating the total number of bacteria. However, the results were highly correlated with the ones gathered from manual counts. *OpenCFU* software was also developed, where the control over the processing parameters is provided and thus could be used in applications in colony counting and other circular objects, yet, the process lacks an higher level of automation [5].

Some of the outlined existent solutions exhibit excellent accuracy results and are seen as potential solutions that contribute to the laboratory automation and efficiency. However, most of them reveal one of two flaws; excessive user-provided action or information, and statistical relevance, expressing the need of being tested in larger and significant databases, resembling the actual and demanding laboratorial environment.

Reference papers on bacteria image classification are more sporadic than quantification systems and are often related to specific clinic applications as proposed in [6], while developing an automated tool to identify bacterial types using computer vision and statistical models. Recently, and combining colony counting with machine learning, in [7] was proposed a deep learning approach based on the design of a Convolutional Neural Network and tested on an extensive database. The obtained results in quantification tasks were very promising and reliable, as a result of the large database. In [8] was designed a system for the classification of foodborne pathogens using image analysis and machine learning tools but assuming that feature-extraction tools on that specific situation would be computationally complex and requiring extensive testing. A complete segmentation, enumeration and classification pipeline with a promising performance has been proposed in [9]; in order to differentiate colonies of different species they adopted a Support Vector Machine (SVM) with Radial Basis Function as the classifier. An SVM approach was also addressed in [10], where a series of three classification steps was employed.

1.3 Objectives and Contributions

The main objective of this work was the development of a software capable of automatically quantifying the number of colonies in Petri-plates. Furthermore, aiming at assembling an intelligent

system capable of both differentiation and automatic detection of the colony type present on the image. There are numerous commercially available instruments that perform plate enumeration with various advantages: saving costs by reducing enumeration time, automatic documentation, reproducibility, and operator independence. However, even with the existent realization of all the advantages of automated image analysis it is necessary to invest in an expensive, high performance commercial system, or to acquire expert knowledge in image processing. These are common obstacles of many laboratories that could be avoided with a cost-effective yet efficient system comparable to the one pursued with the development of this work.

1.4 Dissertation structure

The current dissertation is assembled in six chapters. In the first chapter an introduction is made: the rationale is presented as well as proposed objectives, related existing procedures and the framework of this document. The second chapter addresses the microbiology background essential for the theme. In chapter 3, fundamental concepts related to images, image processing procedures and machine learning approaches are presented. The fourth chapter comprehensively describes the methodology, branched into two segments: the microbiology techniques applied to the database conception and the methods handled on image processing. In the fifth chapter the results of this work are exhibited, and the respective discussion is addressed. The last chapter of this thesis encloses the conclusions of the work and identifies future aspects to improve the obtained results.

CHAPTER 2

Microbial Enumeration

2.1 Methods for Enumeration and Detection of Microorganisms

The basis of much of environmental and clinical microbiology over its history has been learned through the removal and isolation of microorganisms under artificial laboratory conditions from natural environments from which they have adapted. Microorganisms play an important role in life in general, nonetheless it is worthwhile to understand its implications. A substantial way to access these implications is through microbial population monitoring. The enumeration of microorganisms is an important way of accessing the microbial population in many types of samples and consequently many procedures depend on an accurate count of the bacterial colonies and other organisms. Thus, these techniques can be employed in a wide range of fields. If a literature review is made to understand its importance it will be noticeable that these methods are widely used to check the effectiveness of disinfectants, gauge sanitary quality, conduct assays in biomedical examinations, certify that food products meet desirable specifications and also evaluate possible levels of contamination, conduct drug safety evaluations in pharmaceutical industries and evidently, in research, where enumeration methods are employed on a daily basis in laboratories worldwide [11, 12]. Some of the outlined applications of microbial quantification are specified next.

In the food industry, microorganisms are, at the same time, beneficial but also the principal cause of food spoilage. According to the type of microorganism the consequences of food contamination can be both hygienic and financial. Contamination by harmless microorganisms, for example, can cause sensorial defects in products and thus, a loss of their commercial value. These products can also cause severe foodborne diseases, either due to the organisms themselves or to the toxins released by bacteria or molds [13]. In the dairy industry, the increasing number of outbreaks associated with dairy products has highlighted the importance of microbial control and for that this assessment is

essential [14].

In the environmental field, the applications are also vast. The usual concern with the microbiological quality of water is the presence of pathogens and parasites. Very often, the risk of water-borne diseases is evaluated not by the direct presence of pathogens, but by the presence of indicator microorganisms. Flow cytometry and conventional enumeration can be performed and the quantification of active heterotrophic microorganisms in natural waters has also been assessed [15, 16].

Bacterial colony enumeration is likewise an essential and powerful tool in biomedical assays; in dentistry, for example, there are over five hundred bacterial species and several of them have very close relationship with various diseases, such as dental caries and periodontal diseases. Oral samples are collected and cultured in order to quantify the number of bacteria; this diagnosis will help determine the proper antibiotic agents to use clinically [3]. In [17] was also reported the importance of monitoring the microbial population in a hospital environment. In medical microbiology the identification and enumeration of microorganisms is relevant as well, as detailed in [18].

Some methods count colony numbers, other methods measure the population's total mass, which is often directly proportional to cell numbers. Population numbers are usually recorded as the number of cells in a milliliter of liquid or in a gram of solid material. Because bacterial populations are usually very large, most methods of its quantification – described next – are based on direct or indirect counts of very small samples; calculations then determine the size of the total population. When performing an enumeration method, analysts do viable counts and should be reported as Colony Forming Units (CFU), which is equal to the number of colonies on a plate multiplied by the inverse of the dilution of the sample and by the inverse of the amount (volume) of diluted sample plated:

$$CFU/mL = N^o \text{ of colonies} \times \frac{1}{dilution} \times \frac{1}{volume}. \tag{2.1}$$

A viable cell is one that is able to divide and form offspring (the growth of bacterial cultures is addressed in Section 2.2), and in most cell-counting situations, these are the cells analysts are most interested in. For these purposes, one would use a viable cell count, also called a plate count because agar plates are required. The assumption made in a viable count is that each viable cell will grow and divide to yield one colony, and hence, colony numbers are a reflection of cell numbers [11].

2.1.1 Direct Methods

2.1.1.1 Direct Microscopic Count

In several situations, as mentioned previously, the clumps of bacteria found on standard plate counts could lead to underestimation of the number of cells. To overcome that limitation the direct microscopic count may be employed. In this method, a measured volume (regularly 0.01 mL) of a bacterial suspension is spread over a defined area on a microscope slide, stain is added to enable the visualization of the bacteria, and the sample is viewed under the oil immersion objective lens.

The number of bacteria can then be counted. To perform the counting a Petroff-Hausser cell counter or a Neubauer chamber can be used. The Neubauer chamber is the most commonly used in virtue of its broader applications and has a deeper counting layer (0.1 mm) when compared to the Petroff-Hausser counter (with a cell-depth of 0.02 mm), thus, the supported volumes are different. The chief advantage of microscopic counts is that no incubation time is required, thus, these methods are usually reserved for applications in which the time is the primary constraint. On the other hand, the most serious drawback of these methodologies is their inability to distinguish between viable and non-viable bacteria [19]. In addition, a rather high concentration of cells is required to be countable – about 10 million bacteria per milliliter.

2.1.2 Indirect Methods

2.1.2.1 Plate Counts

The plate count is the most commonly used method to gauge bacterial populations. It has an easy-to-follow procedure and shows very accurate results when performed according to good practices. This method was the elected one in the present work, for database creation for posterior image analysis, thus will be examined with more detail, exploring its advantages, limitations and sources of error. An important advantage of this method is that it only considers the number of viable cells. However, it has one substantial disadvantage, usually 24 hours or more are required for visible colonies to form. This can be a considerable limitation in some applications, such as quality control of certain foods and in human samples, e.g. tissue, body fluids, pulmonary secretions, and blood.

This method assumes that each living bacterium cell grows and divides to originate a single colony, which is not always true. Bacteria frequently grow linked in chains or as clumps, consequently, a colony often derives not from a single bacterium but from a segment of a chain or from a clump. In order to illustrate this reality, plate counts are reported as CFUs, as mentioned before.

It is also important to guarantee that a limited number of colonies develop in the plate. Inaccuracies will occur when performing the counting if the plate is overpopulated with colonies, some will not grow because of the limited area. According to the U.S. Food and Drug Administration, plates are considered normal within the range of 25 to 250 colonies. Plates with more than 250 colonies should be reported as too numerous to count (TNTC). However, many microbiologists prefer the range from 30 to 300 colonies per plate. The origin of the mentioned ranges was examined in detail in [20]. To ensure that some colony counts fall into this range, the original inoculum is diluted several times – serial dilution; a process described later in Chapter 4.

According to the literature, the classic enumeration methods are the pour-plate method, the surface or spread plate method, the oval tube or bottle culture method, the plate loop method, drop plate method and the membrane filtration method. However, the most used are the pour-plate and the spread-plate method. Another method of plating is the spiral plating – an automated way of plating – and it is also a spread plating method; it allows the plating of 4 dilutions on the same dish

by spreading a decreasing amount of sample with known volumes throughout the plate. This method follows an Archimedes spiral, logarithmically decreasing from the center of the Petri-plate towards the periphery. The main advantage is related with the spared material as it enables 4 dilutions on the same plate. Otherwise errors or contamination can easily spread [21].

For the pour plate method, either 1 mL or 0.1 mL of the bacterial suspension is introduced into a Petri-plate. The nutrient medium, in which the agar is kept liquid by holding it in a water bath at about 50°C, is poured over the sample, which is then mixed into the medium by gentle agitation of the plate. When the agar solidifies, the plate is incubated. With the pour plate technique, colonies will grow within the nutrient agar (from cells suspended in the nutrient medium as the agar solidifies) as well as on the surface of the agar plate.

This technique has some drawbacks because some relatively heat-sensitive microorganisms may be damaged by the melted agar and will therefore be unable to form colonies. Also, when certain differential media are used, the distinctive appearance of the colony on the surface is essential for diagnostic purposes. Colonies that form beneath the surface of a pour plate are not satisfactory for such tests. To avoid these problems, the spread plate method is frequently used instead; here 100 μL of the inoculum is added to the surface of a prepared, solidified agar medium. The inoculum is then spread uniformly over the surface of the medium with a specially shaped, sterilized glass or metal rod. This method positions all the colonies on the surface and avoids contact between the cells and melted agar [12].

The number of colonies obtained in a viable count experiment depends not only on the inoculum size and the viability of the culture, but also on the culture medium and the incubation conditions. The colony number can also change with the length of incubation. For example, if a mixed culture is counted, the cells deposited on the plate will not all form colonies at the same rate; if a short incubation time is used, fewer than the maximum number of colonies will be obtained. Furthermore, the size of colonies may vary. If some tiny colonies develop, they may be missed during the counting. With pure cultures, colony development is a more synchronous and uniform process. As mentioned previously, microbial cells often occur as clumps; while shaking and performing dilutions of the sample tends to uniformly distribute the clumps of bacteria, these procedures may not completely disrupt them and ensure that the microorganisms will be distributed as single cells.

When considering the entire procedure and the results obtained, precision and accuracy are important, once similar results in repetitive counts (made by the same person or other analysts) and the lowest difference possible from the "true" count are required. The accuracy of the colony count method may be limited by the failure of some microorganism to form visible colonies on the agar media; occasionally, these microorganisms do not grow in culture media but are still metabolically active and capable of causing infections, they are said to be in a viable but nonculturable cell state (VNBCs). Traditional laboratory culture conditions and methods cannot meet the requirements of VNBC organisms to resume growth. These cells exhibit active metabolism in the form of respiration or fermentation, incorporate radioactive substrates, and have active protein synthesis but still cannot

be cultured or grown on conventional media [22]. VNBC cells may be a problem in the environment if they are pathogens, i.e. viable but nonculturable cells of *Vibrio cholerae*, enteropathogenic *E. coli*, *Legionella pneumophila*, among others. Some of these have been shown to regain culturability after they have entered the intestinal tracts of animals [23].

Additionally, other microorganisms besides VNBCs can be underestimated by the colony count method. This failure can result from nutritional deficiencies of the medium, inaccurate pipetting of a liquid sample, unfavorable oxygen tension, unfavorable incubation temperature, cell injury, nonuniform sample, insufficient mixing and other factors. The presence of inhibitory substances on glassware or in diluents or produced by competitive microorganisms in the agar may adversely affect some microbial cells and limit their availability to form colonies.

Another factor that affects apparent counts is the analyst's ability to see colonies distinctly. This depends on colony separation and morphology. Procedures that enhance colony growth and improve size, shape, contrast, and distribution should be used. The analyst's eyesight and fatigue may reduce the reliability of the count. Other factors which may influence the accuracy of the colony count include: improper sterilization and protection of sterilized diluents, media, and equipment, inaccurate measurement of sample and dilutions, improper distribution of the sample in or on the agar medium, unsatisfactory working areas that permit contamination. Aditionally, erratic mixing or shaking of sample or dilution, inaccurate determination of colonies due to the presence of artifacts such as small particles and scratches on plates, improper evaluation of spreaders or pinpoint colonies, or other error in counting and in computing counts.

Summarily, while there are some inherent limitations in enumerating microorganisms by the colony count method, most of the errors can be minimized if the analyst follows directions carefully and exercises extreme care in making all measurements. Consistently accurate and meaningful results can be obtained from the routine examination using the same methods or procedures. This includes sampling procedures, sample preparation, preparation of dilutions, plating medium, incubation conditions, and counting procedures.

2.1.2.2 MPN-Most Probable Number

Another method for determining the number of bacteria in a sample is the most probable number method. The MPN method permits estimation of population density without performing a count of colonies. It is sometimes called the method of ultimate or extinction dilution or, in a simpler definition, the dilution method. The MPN technique is based on a determination of the presence or absence of microorganisms in several individual portions of each of several consecutive dilutions of the sample under analysis. On the basis of the probability theory, it is possible to estimate, from the numbers of positive and negative tubes receiving a certain quantity of inoculum, the most probable number of microorganisms in that quantity of inoculum. By further elaboration of the theory, it is possible to combine the results from different dilutions in such a way that a single value is obtained

for the most probable number of a given microorganism [24]. A general equation for calculating the MPN in successive dilutions was developed in [25].

The MPN method is most useful when the microbes being counted will not grow on solid media. It is also useful when the growth of bacteria in a liquid differential medium is used, like in the identification of coliform bacteria, in water testing.

2.1.2.3 Membrane Filtration

The bacterial populations can as well be determined by passing a sample trough a membrane filter – membrane filtration – when the quantity of bacteria is considerably small. Thus, the bacteria are filtered out and retained on the surface of the filter. The membrane is then transferred to a Petri-plate containing nutrient medium, where colonies will grow and form visible colonies. At the beginning this method was only applied to high-value products, however, membranes have subsequently developed into a cost-efficient and robust tool for separation of different phases, thus, started to be applied in areas such as biomedicine, biotechnology and biopharmacy [26].

The primary advantage of filtration over conventional spread plating is its low detection limit and the ability to test large amounts of samples. Incubation time for visible colony formation varies from 18 hours to up to several weeks, depending on the organism of interest, the origin of the sample and the growth media employed [27]. This characteristic could potentially be a disadvantage of the method, when compared to the standard plate count.

2.1.2.4 Turbidity

This method is seen as a practical approach of monitoring bacterial growth and assuming that the bacteria proliferate in a liquid medium, the medium becomes turbid, or cloudy with cells. A spectrophotometer is required to accomplish the measurement; a beam of light is transmitted through a bacterial suspension to a light-sensitive detector. The amount of light striking the detector will be inversely proportional to the number of bacteria. Based on the Beer-Lambert Law, two metrics are displayed in the instrument, the transmittance and the absorbance (a logarithmic expression), also referred to as optical density. The absorbance can be used to plot bacterial growth and if the readings are matched with plate counts of the same culture, this correlation could be used in future estimations of bacterial numbers obtained through measuring turbidity. A limitation is expected related to the detection limits, low concentrations might not be detected (e.g. investigating possible sample contaminations) and on other hand, high concentrations could eventually lead to the saturation of the detector and consequently produce inaccurate measurements.

2.1.2.5 Metabolic Activity

Another indirect way to estimate bacterial numbers is to measure the metabolic activity of the bacteria present in a given sample. Despite possible and recognizable error, this method speculates

that the amount of a metabolic product, like acid or CO_2, is in direct proportion to the number of bacteria present. This method is applicable when bacteria lose culturability but retain measurable metabolic activity and are considered viable. This has led to the concept of VNBCs bacterial cells (adressed in Section 2.1.2.1), while these cells are incapable to form offspring, (required for growth) metabolic activity can be measured [28].

2.1.2.6 Dry Weight

Microbial biomass is a fundamental variable in microbiological research. Expressed as dry weight, the biomass is a parameter that may be required for the determination of growth kinetics, yield factors or metabolic quotients [29]. When filamentous bacteria and molds are intended to be measured, the mentioned method is also suitable, other usual methods are considerably less satisfactory. In this routine, the bacteria are removed from the growth medium and filtered to remove extraneous material. This procedure generally requires lengthy drying phases as well as an equilibration step where the sample temperature is reduced to room temperature in a desiccator, prior the weighting of the product. Accordingly, results are not rapidly available to allow prompt utilization of biomass-based information, which would represent a disadvantage when compared to other methods. Novel methodologies were reviewed in [30] to improve the performance of the said method. In [30], probe technologies are described: dielectric spectroscopy, optical density, infrared spectroscopy, and fluorescence. The general requirements for a reliable probe suited to a wide range of applications are quite demanding; possibility of calibration, linear dependency, precision at both low and high cell density, sterilizable, endure temperature and pressure, corrosion stable and biological inactive. Furthermore, these sensors should also be able to maintain the aforementioned characteristics, over multiple cycles and practices. A brief summary of the applications, advantages and limitations is presented in Table 2.1. Additionally, calculation methods in biomass estimation were summarized in [30]; correlation methods, which often require Stoichiometric coefficients and modeling skills, and software sensors, mathematical models based on growth kinetics, statistical analysis [such as multilinear regression (MLR) and principal component analysis (PCA)], neural networks, or combinations of all of these.

Table 2.1: Probe technologies summary. Adapted from [30].

Method	Interface			Application		
	Solids	Gas Bubles	Conductivity	Single cell suspensions	Filamentous	Immobilized
Optical density	+	t[a]	−	+	t	−
Dielectric spectroscopy	−	−[b]	−[a]	t	+	+
Infrared spectroscopy	+	+[c]	−	+	t	−
Fluorescence spectroscopy	t	t	−	+	+	+

\+ significant interference or possible applicability, − no significant interference or not applicable,
t testing required for every specific case;
[a] depends on the probe type used;
[b] no interference of gas bubbles when dual frequency measurement is used;
[c] with optic fiber probes path length affects the amount of interference.

2.1.3 Advantages and disadvantages of Classic Enumeration Methods

Several advantages and disadvantages of each outlined method are summarized ahead. However, for Classic Enumeration Methods and after a profound literature review, there are some general considerations that need to be highlighted. The most important positive features of these Methods are the ability to recognize viable cells, the high sensitivity when cultivated with appropriate media, the morphological characterization and fundamentally, the monetary cost of performing these kinds of methods, which is much smaller when compared to Rapid Microbiological Methods (RMMs). Thus, the return of the investment (ROI) of a Laboratory that embraces classic methods will be much smaller. On the other hand, there are inevitable disadvantages. The biggest one is related with time; days might be required for the results to be obtained, as e.g. enunciated by Moldenhauer, sterility and mycoplasma testing are often cited as the most serious offenders, with a minimum 14- or 28-day release time, respectively [31]. Significant costs are associated with holding the product this long, which adds to the overall costs of performing Classic Enumeration Methods. Other disadvantages can be mentioned; the required resources, and the fact that a high skill level is necessary to obtain optimal results, once it relies on phenotypic biochemical characterization.

As the clinical microbiology laboratory slowly enters into the new era of "molecular diagnostics", the dependency on traditional culture methods and consequently Classic Enumeration Methods will continue to play an integral role in detecting and characterizing microorganisms. Furthermore, the major goal of the clinical microbiology laboratory has not changed, as stated by Dr. Raymond Bartlett – one of the important microbiologists who influenced clinical microbiology laboratories' standard operating procedures. He stated that the main objective of a clinical microbiology facility is to provide information of maximal and epidemiological usefulness as rapidly as possible, consistent with acceptable accuracy and minimal cost [32]. The two mentioned criteria by Dr. Bartlett explain the slow introduction/acceptance by the clinical microbiology community of non-cultural enumeration methods and continued use of classic methods. RMMs remain cost prohibitive for many laboratories and are not practical or adaptable for use in the service-oriented clinical laboratory. Until such problems are resolved, microbiologists will continue to use classic enumeration methods [32].

2.2 Growth of Bacterial Cultures

2.2.1 Reproduction and Growth Cycle

Microbial cells have a finite lifespan and a species is maintained only as a result of a continuous growth of its population. The most used process in bacteria to obtain growth is binary fission, where, in most cases cells elongate to approximately twice their original length and then form a partition that constricts the cell into two daughter cells. This partition is called a *septum* and results from the inward growth of the cytoplasmic membrane and cell wall from opposing directions; the formation of the mentioned structure continues until the two daughter cells are pinched off. After this process

is completed, one generation has occurred and the required time for that to develop is called the *generation time*. During one generation, cells are in balanced growth, i.e. all cellular constituents increase proportionally. The DNA molecule is also replicated and assigned to each daughter cell, during the *constriction* step, each cell will then receive a chromosome and sufficient copies of ribosomes as well other macromolecular complexes, monomers and inorganic ions to exist as an independent cell. The *generation time* for a given bacterial species is highly variable and is dependent on nutritional and genetic factors. As expected, this rate can also alter from laboratory conditions to the natural habitat environment, as other microorganisms coexist and sometimes competition for resources and space exists [11].

Less frequently and in particular situations, certain bacteria produce endospores – a specialized dormant cell that forms within the bacteria and highly resistant to agents that would normally harm a vegetative cell, such as heat, solvents and ultraviolet radiation. A modified form of binary fission is a fundamental morphological event that marks entry into the endospore formation pathway, but instead of dividing at midcell, a sporulating cell divides near one pole. During the mentioned asymmetric cell division, a prespore and a large mother cell are produced; approximately one-third of one of the chromosomes is trapped in the prespore and the rest of the chromosome is pumped into the smaller cell by the action of a DNA translocase protein. The other copy of the chromosome is retained in the mother cell [33].

A few bacterial species reproduce by budding; a small initial outgrowth is formed and enlarges until its size approaches that of a parent cell, and then it separates. Some filamentous bacteria reproduce by producing chains of conidiospores – an asexual spore – carried externally at the tips of the filaments. A few filamentous species simply fragment, and the fragments initiate the growth of new cells. *Proteobacteria* such as *Pedomicrobium* and *Ancalomicrobium* are examples of bud-producing bacteria, although each has a distinct morphology and pattern of bud formation [33].

As outlined previously, during cell division one cell becomes two and during the *generation time* both total number and mass double. The growth can predictably become exponential and can be expressed with simple mathematics based on a geometric progression of the number 2 (first generation – 2^1; n^{th} generation – 2^n). A fixed relationship exists between the initial number of cells in a culture and the number verifiable after a period of exponential growth. The final cell number thus, can be expressed as:

$$N = N_0 \cdot 2^n \tag{2.2}$$

where N is the final cell number, N_0 is the initial number and n is the number of generations. The generation time of the population is t/n, where t is the duration of the exponential growth (expressed in days, hours or minutes). Consequently, from the initial and final cell numbers it is possible to calculate n, and knowing n and t it is possible to obtain the *generation time*. By taking the logarithms,

the previous equation can be written in order of n:

$$\log N = \log N_0 + n \cdot \log 2 \tag{2.3}$$

thus,

$$n = 3.3 \cdot (\log \mathrm{N} - \log N_0) \, . \tag{2.4}$$

The knowledge of the prementioned parameters is useful for optimizing culture conditions for a newly isolated microorganism and also for testing the positive/negative effect of some treatment on a bacterial culture.

Considering an organism growing in a confined vessel e.g. a tube or flask, the exponential growth will not occur indefinitely, due to lack of area or nutrient depletion. A characteristic growth curve is presented in Figure 2.1, where the distinct stages of the growth cycle are displayed – *lag*, *exponential*, *stationary* and *death phases*.

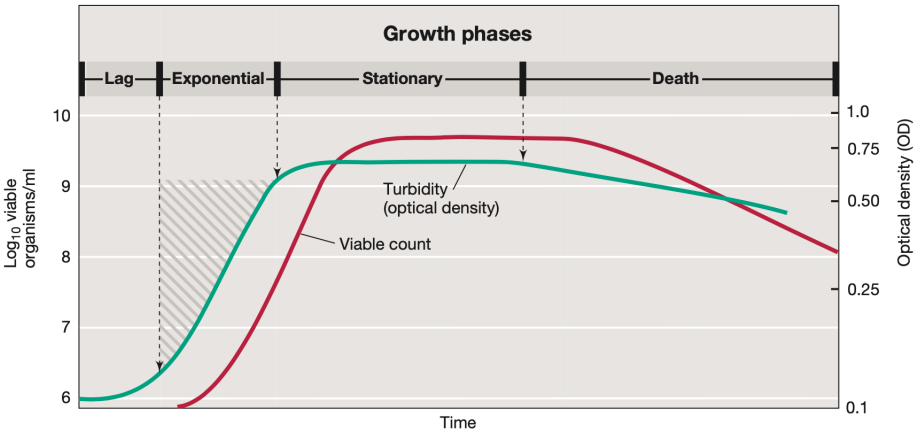

Figure 2.1: Typical growth curve for a bacterial population. Adapted from [11].

After inoculation into fresh media, growth begins only after a certain time, designated by *lag phase*. During this time, however, cells are not dormant. The population is undergoing a period of intense metabolic activity, particularly the synthesis of enzymes and other molecules – creating conditions for exponential development.

Eventually, the cells begin to divide and enter an exponential growth stage – the *log phase*. Cellular reproduction is most active during this period and *generation time* reaches a constant minimum. This step is the time when the cells are most metabolically active and is preferred for viable counts or industrial purposes, where, for example, a product must result from an efficient process.

If the exponential growth continued unchecked, startlingly large numbers of cells could arise. For example, a single bacterium (at a weight of 9.5×10^{-13}g per cell) dividing every 20 minutes – as occurs with *E. coli* – could, in just some hours, develop a population of tons. As a matter of fact, this does not materialize; the growth rate slows, the number of microbial deaths balances the number of new

cells and the population stabilizes. Exhaustion of nutrients, accumulation of waste products and harmful changes in pH support the balanced state. This period of equilibrium is called the *stationary phase*.

Eventually, the population will enter the *death phase* of the cycle, which, like the *exponential phase*, occurs as an exponential function (displayed in Fig. 2.1). Typically, however, the rate of cell death is much slower than the rate of exponential growth and viable cells may remain in a culture for months.

The described cycle is a reflection of populations, not individual cells. Which actually is most relevant to the ecology of microorganisms because measurable microbial activities require populations [11].

2.2.2 Media

Cultural methods are based upon providing a combination of nutritional and physicochemical conditions that will support the growth of the microorganisms of interest. Most of the media, which are available from commercial sources, have premixed components and require only the addition of water and then sterilization [12]. The major nutritional requirements for microbial growth that must be considered are sources of carbon, sources of energy, electron acceptors, nitrogen sources, sources of nutrients (such as sulfur, phosphate, magnesium, and calcium), vitamin requirements and trace metal requirements. Some physicochemical factors affecting growth include temperature, pH, requirement for oxygen, and salinity [11].

The range of media developed to culture bacteria reflect their nutritional versatility and range of growth conditions tolerated, thus, depending on the purpose and the microorganism, different types of media can be selected, as found on Table 2.2. It is possible to access a wide variety of both classic and modern media used for the identification and maintenance of diverse bacteria medically important in the *Handbook of Media for Clinical and Public Health Microbiology* [32].

Table 2.2: Types and purposes of culture media. Adapted from [12].

Type	Purpose
Chemically Defined	Growth of chemoautotrophs; microbiological assays
Complex	Growth of most chemoheterotrophic organisms
Reducing	Growth of obligate anaerobes
Selective	Suppression of unwanted microbes; encouraging desired microbes
Differential	Differentiation of colonies of desired microbes from others
Enrichment	Similar to selective media but designed to increase numbers of desired microbes to detectable levels

2.2.2.1 General Media

The General-purpose media are extensively used on microbiological practices as they enable the growth of a wide variety of microorganisms. The offered set of nutrients and conditions by these media meet the required criteria of many microorganisms to grow. Hence, these media have low specificity and selectivity.

2.2.2.2 Selective Media

In clinical and public health microbiology, it is frequently necessary to detect the presence of specific microorganisms associated with disease or poor sanitation. For this task, selective media are used. Selectivity refers to the media's ability to primarily support only the growth of the target microorganism and to minimize interfering background growth.

Because bacteria present in small numbers can be missed, especially if other bacteria are present in much larger numbers, it is sometimes necessary to use an enrichment culture. This culture can be applied to favor a specific microorganism or to recover one from a mixed culture. Improved recovery can sometimes be obtained from the selective phase because of the primary, benign enrichment step. Medium components are used to provide selectivity by inhibiting growth of unwanted species; these may include organic compounds such as bile salts and sodium deoxycholate and inorganics, such as sodium selenite and sodium tetrathionate [34].

There are many selective media available, e.g., Hektoen enteric agar (HE) which is selective for Gram-negative bacteria and Bile Salt Agar which is selective for *Vibrio cholerae*. A selective medium can as well be designed to increase very small numbers of the desired type of organism to detectable levels.

2.2.2.3 Differential Media

These media contain compounds that allow groups of microorganisms, grown on the same tube or plate, to be visually distinguished by the appearance of the colony or the surrounding media, usually on the basis of some biochemical difference between the two groups. Blood agar is a medium that microbiologists frequently use to identify and distinguish bacterial species through the type of hemolysis produced. For example, *Streptococcus pyogenes*, when grown on blood agar shows a clear ring around their colonies, areas where red blood cells (RBCs) are lysed through β-hemolysis. Mannitol salt agar is a media that combines both features of differentiating and selecting; it is differential because some bacteria are capable of fermenting the mannitol (e.g. *S. aureus*) in the medium which will cause it to change color, causing differentiation. On the other hand, this medium is also selective due to the high salt concentration that prevents the growth of several bacterial species [12].

CHAPTER 3

Image Processing and Artificial Inteligence

3.1 Digital Image

An image may be defined as a two-dimensional continuous function, $f(x,y)$, where x and y are spatial coordinates, and the amplitude of f at any pair of coordinates (x,y) is called the intensity or gray level of the image at that point. When x, y and the intensity values of f are discrete quantities, the image is called a digital image, which is essentially a two-dimensional ordered matrix of integers assuming a discrete representation of data. Thus, a digital image is composed of a finite number of elements with a single location and value. These elements are called pixels [35–37].

3.1.1 Image sensing, acquisition and digitization

Regarding image sensing and acquisition, most of the images are generated by the combination of an "illumination" source and the reflection or absorption of energy from that source by the elements of the "scene" being imaged. The illumination originates from a source of electromagnetic energy, ranging all the bands in the electromagnetic (EM) spectrum. As the source of illumination ranges from traditional sources (e.g. radar, visible, infrared) to less traditional ones (ultrasound, computer-generated illumination pattern), the scene elements could be familiar objects, but they can just as easily be molecules, buried rock formations or a human brain. Depending on the nature of the source, illumination energy is reflected from, or transmitted through, objects. In Figure 3.1a is shown a single sensing element, used to transform incident energy in digital images; incoming energy is transformed into a voltage by a combination of the input electrical power and a sensor material that is responsive to the type of energy being detected. The output voltage waveform is the response of the sensor, and a digital quantity is obtained by digitizing that response. There are three principal sensor arrangements, single element (Fig. 3.1a), line and array [35–37]. Other types of image sensors

can be found in specialized camera products, particularly hexagonal elements – approached with detail in [38], and circular sensor structures, recently employed in [39] to obtain an high performance sensing system. Image formation can be seen as a process (Fig. 3.1b) which transforms an input distribution into an output distribution and the lens may be viewed as the responsible *system* for the transformation process. In Figure 3.1c, the process of digitization is evidenced, where the continuous signal is converted into its discrete representation.

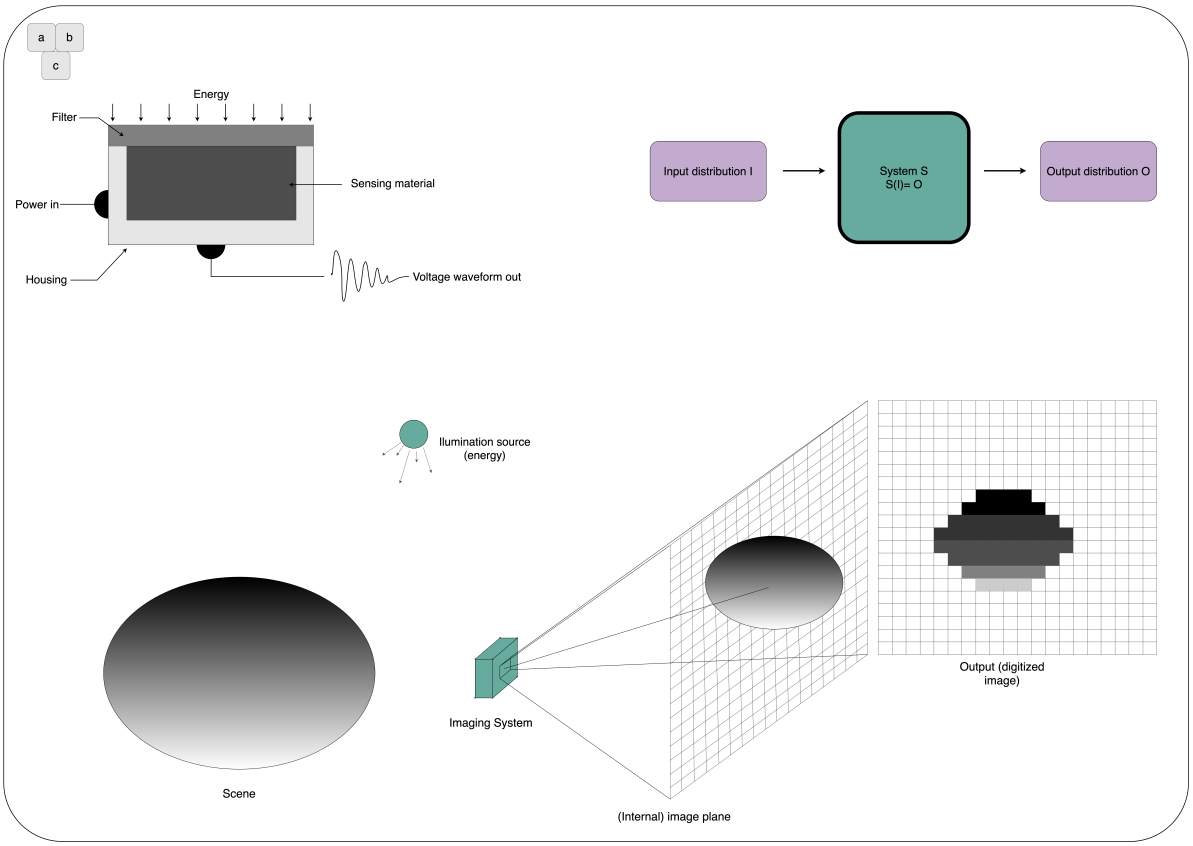

Figure 3.1: Image sensing, acquisition and digitization. (a) a single sensing element is represented; (b) image formation process and (c) an example of digital image acquisition. Adapted from [35].

3.1.2 Image Filtering and Enhancement

Images are the essence of vision and relatively to this project, images are the core data to be studied. There are several ways – from simple to sophisticated – for processing and analyzing them. As raw data, images frequently require filtering which involves the application of window operations that perform useful functions, such as noise removal and image enhancement. The basic goal of these processes is the best possible assessment of visual information, with logical but crucial condition; the desired information to be extracted, emphasized or restored must exist in the image. Several of

these operations apply the local neighborhood concept, where pixel values are influenced by adjacent pixels [40]. Respecting linear filters, the value of a certain pixel is obtained through linear combinations among the neighbor pixels and that linear combination is called a *kernel* or a *mask* – an array of exactly the same size as the selected neighborhood containing an anchor point at the center. A filtering procedure is implemented by successively positioning the center of the mask coinciding with each target pixel. The *mask* then 'slides' over the image (or the region of interest to be processed) multiplying the pixels underneath the *mask* by the corresponding weights w, obtaining the new values by summing the total and assigning them to the same location in a new (filtered) image. The described procedure is called convolution. The convolution between a *mask* and an image, addressing the row and column indices of both *mask* and image, can be expressed as:

$$f_{conv}(x,y) = \sum_{i=I_{min}}^{I_{max}} \sum_{j=J_{min}}^{J_{max}} w(i,j) \cdot f(x+i, y+j) \tag{3.1}$$

where, w corresponds to the kernel values and the indices $i = 0,\ j = 0$ correspond to the center of the kernel, with size $(\ I_{max} - I_{min} + 1,\ J_{max} - J_{min} + 1)$.

The removal of noise or the sharpening of image edges are examples of common enhancement techniques and according to [41], noise reductions are commonly classified into two classes, linear and non-linear techniques. While performing linear techniques, noise reduction formula is linearly applied to all pixels of image without classifying pixels into noisy and non-noisy pixels. Some drawbacks of linear algorithms are related to damaging the noise-free pixels once the algorithm is applied on both noisy and noise-free pixels. Otherwise, non-linear procedures can sometimes overcome the mentioned limitation in a non-linear-filter-characteristic approach: first the noise is detected and secondly, only the detected (noisy) pixels are replaced by the estimated value. In [42] noise reduction techniques were extensively reviewed and different algorithms were tested on MRI and space images.

3.2 Filtering and Enhancement

3.2.1 Median Filter

The median filter is a non-linear and order-statistical spatial filter. Firstly, this filter's main objective is to examine the local intensity distribution within a particular neighborhood, find the extremes of that distribution – which are likely to have arisen from impulse noise – and subsequently generate a new image corresponding to the set of median values where every pixel image will be replaced by the median of the pixels in the corresponding filter region (R):

$$f'(x,y) \leftarrow \textit{median}\,\{f(x+i,\ y+j)\,|\,(i,j) \in R\}\ . \tag{3.2}$$

The median filter can be considered one of the most widely used filters in general image processing applications; it is superior to the mean filter at preserving sharp high-frequency detail (i.e. edges) whilst also eliminating noise spikes, such as salt and pepper noise. There are discussions about the computation time of this filter however it has been noticed that on proceeding from one *mask* to the next, relatively few new pixels are found, meaning that the new median value can be updated with the old one, therefore saving computation time [43]. The shifts introduced by median filters can be found in detail in [40].

3.2.2 Morphological Operations

Most of these techniques are applied in object isolation, removing considerable noise in the image and connecting segments that belong to the same object. These transformations are applied to binary and intensity images and are also used in procedures to obtain gradient adjustment. Two of the most widely used operations are the dilation and erosion processes, employed in noise suppression and even in some irregular object contours.

3.2.2.1 Dilation and Erosion

Regarding morphological operators, they achieve their purposes by probing the image itself with another set of known shapes called *structuring elements* (SE). The shape of the SE is usually chosen according to some prior knowledge about the geometry of relevant and irrelevant image structures. Dilation is a process that results from the intersection of the image with a *mask*. In an intensity image, the effect of the *mask* is similar to a local maxima operator. From the overlapped pixels by the SE the central value is replaced with the maximum value founded:

$$\delta_B(x) = \max_{\beta \in B} f(x+\beta) \tag{3.3}$$

where β are the vectors of B and subsequently adding to the object the pixels of the background that touch the object. Having B as a SE, dilation can formerly be described as:

$$\delta_B = \{x \,|\, (\hat{B})_x \cap f(x,y) \neq \emptyset\} \,. \tag{3.4}$$

This operator is frequently applied when a certain object is fragmented; in this situation the aim is to connect the regions with similar intensities. When performing erosion, the SE slides along the image and the minimum pixel value is obtained from of the pixels overlapped by the structuring element:

$$\varepsilon_B(x) = \min_{\beta \in B} f(x+\beta) \tag{3.5}$$

afterwards the obtained value is attributed to the central pixel, removing from the object the pixels of the edges. In a binary image, for pixels to be considered for the operation, the intersection of

the image and the *mask* has to be the *mask* itself. This operation is frequently used to erode small segments in an image and at the same time preserving in this way the significant content of the image. Some more detailed mathematical definitions of both transformations can be found in [36].

Opening and closing operators are processes enabled by the combinations of dilations and erosions. The opening operator is widely handled in region enumeration where an erosion is followed by a dilation. Thus, the opening γ of an image f by a *structuring element* B can be denoted as $\gamma_B(f)$ and defined as the erosion of f by B followed by the dilation with the reflected SE, $\check{B}$:

$$\gamma_B(f) = \delta_{\check{B}}[\varepsilon_B(f)] \tag{3.6}$$

i.e., $\gamma_B(f) = \delta_{\check{B}} \cdot \varepsilon_B$. It is also possible to formulate the opening in terms of SE fit, given that an erosion corresponds to an intersection of translations of the SE over the image. Therefore, the opened set is the union of all SEs fitting the set:

$$\gamma_B(X) = \bigcup_x \{B_x \,|\, B_x \subseteq X\} \,. \tag{3.7}$$

In the opposite way, the closing operator is performed by a dilation followed by an erosion. Same as the formulation of the opening and assuming $\phi_B(f)$ as the closing operation of an image f, the process can be described as:

$$\phi_B(f) = \varepsilon_{\check{B}}[\delta_B(f)] \tag{3.8}$$

i.e., $\varepsilon_{\check{B}} \cdot \delta_B$. Using the set notation, and considering again the intersection of all translations of the complement of B it is possible to denote:

$$\gamma_B(X) = \Big[\bigcup_x \{B_x \,|\, B_x \subseteq X^c\}\Big]^c \tag{3.9}$$

admitting that the SE fit the background of the set. This procedure is commonly used to fill segments and to reduce certain noise in the image [35–37].

3.2.2.2 Top-Hat Transformation

Combining subtraction with openings and closings results in a *top-hat* transformation which can be defined, in a grayscale image f, as the image *minus* its opening:

$$T_{\textit{top-hat}}(f) = f - \gamma_f \,. \tag{3.10}$$

One of the principal applications of this transform is in removing objects from an image by using a structuring element in the opening operation that does not fit the objects to be removed. The difference operation than yields an image in which only the removed components result. This

transformation is normally applied for light objects on a dark background, for this reason, this transformation is frequently called *white top-hat* [35].

3.2.2.3 Regional Extrema and H-extrema Transformations

Image minima and maxima are important morphological features because they often mark relevant image objects: minima for dark objects and maxima for bright objects. In morphology, the term minimum is used in the sense of regional minimum, i.e., a minimum whose extent is not necessarily restricted to a unique pixel. Denoting M as a regional minimum of an image f at elevation t, the mentioned feature can be defined as a connected component of pixels with the value t whose external boundary pixels have a value strictly greater than t:

$$f(x) = \begin{cases} \forall p \in M, & f(p) = t\,; \\ \forall q \in \delta^{(1)}(M) \setminus M, & f(q) > t\,. \end{cases} \tag{3.11}$$

Similarly, the same logic is applied when referring to a regional maximum of an image whereas external boundary pixels have a value strictly less than t:

$$f(x) = \begin{cases} \forall p \in M, & f(p) = t\,; \\ \forall q \in \delta^{(1)}(M) \setminus M, & f(q) < t\,. \end{cases} \tag{3.12}$$

Regional extrema of an image can be defined as the union of its regional minima and maxima. According to Equation 3.13, the set of all maxima of an image f at level t corresponds to the connected components of the cross-section of f at level t ($CS_t(f)$) that are not connected to any component of the cross-section of f at level $t+1$. Consequently, they are not reconstructed by the morphological reconstruction, MR, by dilation of $CS_t(f)$ from $CS_{t+1}(f)$. A regional maxima declared as $RMAX_t(f)$, is:

$$RMAX_t(f) = RMAX(f) \cap T_t(f) = CS_t(f) \setminus MR^{\delta}_{CS_t}(f)\,[CS_{t+1}(f)]\,. \tag{3.13}$$

Following the previous concept, the regional minima, $RMIN_t(f)$, can be denoted as:

$$RMIN_t(f) = RMIN(f) \cap T_t(f) = R^{\varepsilon}_{CS_{t+1}}(f)\,[CS_t(f)] \setminus CS_{t+1}(f)\,. \tag{3.14}$$

Given that regional extrema can occasionally be irrelevant, h-extrema transformations manage to be an useful tool to filter the image extrema using a contrast criterion; h-maxima transformation suppresses all maxima whose depth is lower or equal to a given threshold level h, achieved by a reconstruction by dilation of f from $f-h$:

$$HMAX_h(f) = R^{\delta}_f(f-h)\,. \tag{3.15}$$

By analogy, the h-minima transformation can be defined as:

$$HMIN_h(f) = R_f^{\varepsilon}(f+h). \tag{3.16}$$

Due to the addition or subtraction of the constant h, all the previous transformations must be carefully applied in order to avoid data overflows. The extended minima/maxima, $EMIN$ and $EMAX$, respectively, are defined as the regional extrema of the corresponding h-minima transformation, being defined as follows:

$$EMIN_h(f) = RMIN\left[HMIN_h(f)\right], \tag{3.17}$$

$$EMAX_h(f) = RMAX\left[HMAX_h(f)\right]. \tag{3.18}$$

The reason for these extrema, consists in the fact that if an original extremum is still belonging to an extremum of the reconstructed image, its spatial extent is either unchanged or extended due to the reconstruction procedure. Thus, the total number of extended extrema can only decrease when the value of h increases [35–37, 44].

3.2.2.4 Intensity Transformation – Constrast Adjustment

Low-contrast images can result from poor illumination, lack of dynamic range in the imaging sensor, or even the wrong setting of a lens aperture during image acquisition. When performing these operations, the aim is to expand the range of pixel intensity levels in an image so that it spans the ideal full intensity range of the recording medium or display device. The contrast adjustment procedure can be addressed by *contrast stretching*, also known as normalization. To perform stretching, the upper and lower limit pixels are needed to be found, denoted as a and b, respectively. These are generally the upper and lower limits of the pixel quantization range in use (i.e. a=255 and b=0, for an 8-bit image) The first part of the contrast stretch operation is made by scanning the input image to obtain the maximum and the minimum pixel values currently present, denoted as c and d, respectively. Based on these four parameters, the image pixel range is stretched according to:

$$f_{output}(x,y) = (f_{output}(x,y) - c) \cdot \left(\frac{a-b}{c-d}\right) + a\,, \tag{3.19}$$

for each pixel location denoted by (x,y) in the input and output images [37, 45].

3.3 Image Segmentation and Analysis

The segmentation of an image can be defined as its division into different regions, each having certain properties. In a segmented image, the elementary picture elements are no longer the pixels but connected sets of pixels. Image segmentation is therefore a key step towards the quantitative

interpretation of image data. The design of an algorithm for segmenting an image into meaningful regions requires some prior knowledge about the image objects that are to be recognized [44]

3.3.1 Watershed Transform

The fundamentals of the Watershed method have been developed during the last decades and today is one of the most implemented techniques in cell segmentation models. To separate agglomerated objects is one of the most complex tasks in image processing because segmentation accuracy determines the success or failure of computerized analysis procedures [35]. The basic process of the Watershed method and the first steps towards the model creation were intuitively addressed in [46]. Originally the Watershed method derived from topology: the term watershed refers to a ridge that divides areas drained by different river systems and a catchment basin is the geographical area draining into a river or reservoir. The key behind using this transform for segmentation is changing the desired image into another whose catchment basins are the objects to be identified.

3.3.1.1 Morphological gradient

One of the main segmentation criteria is related with the homogeneity of intensities from specific objects in an image. Hence, gradient is frequently used in Watershed transformations [47]. The morphologic gradient of an image (ρ_B), also defined as Beucher gradient, is obtained through the algebraic difference between a dilation and an erosion by a *structuring element* B [48]. It can be described as:

$$\rho_B = \delta_B - \varepsilon_B \tag{3.20}$$

where δ_B and ε_B are, respectively, elementary operations of dilation and erosion. From the latter equation, it is verifiable that ρ_B outputs the maximum variation of the grey level intensities within the neighborhood defined by B rather than a local slope. If a continuous case is assumed, the gradient can be defined as follows:

$$\rho_B = \lim_{\lambda \to 0} \frac{\delta_{B_\lambda} - \varepsilon_{B_\lambda}}{2\lambda} \tag{3.21}$$

where B is a *disk element* whose radius λ tends to zero.

3.3.1.2 Distance function and geodesic distance

When the geometric shape of an object is one of the main criteria on segmentation processes, the distance function can be fairly useful. Let A be a set which is first supposed to be connected. The geodesic distance $d_A(p,q)$ between two pixels p and q in A is defined as the length L of the shortest

path(s) $P = (p_1, p_2 \ \ldots, p_l)$ linking p and q and included in A (Figure 3.2a):

$$d_A(p,q) = \min\{L(P) \,|\, p_1 = p,\, p_l = q,\, \textit{and}\ P \subseteq A\}\ . \tag{3.22}$$

The set A is referred to as the *geodesic mask*. The paths of minimal length are called *geodesics*. Similarly, the geodesic distance between a pixel p of A and a subset Y of A, $d_A(p,Y)$, is the smallest geodesic distance p and any pixel q of Y (Fig. 3.2b):

$$d_A(p,Y) = \bigwedge_{q \in Y} d_A(p,q)\ . \tag{3.23}$$

The set Y is referred to as the marker set. Both geodesic paths previously described are followingly illustrated:

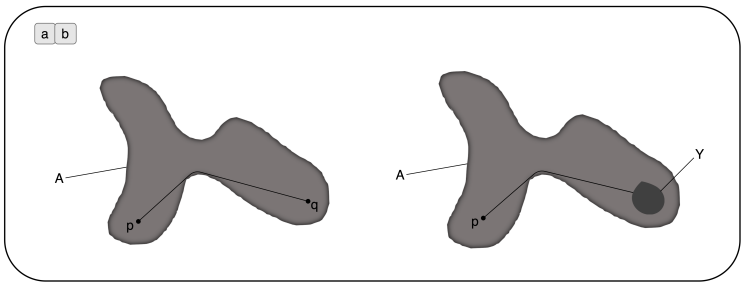

Figure 3.2: Geodesic pathways; (a) between two points and (b) between a point and a set. Adapted from [47]

The geodesic skeleton by influence zone (Fig. 3.3) derives directly from the definition of the geodesic distance and is at the basis of the definition of the watershed transformation. Let X be a set composed of the union of connected components K_i and included in a larger connected set A. The geodesic influence zone $IZ_A(K_i)$ of a connected component K_i of X in A is the locus of points of A whose geodesic distance to K_i is smaller than their geodesic distance to any other component of X:

$$IZ_A(K_i) = \{\, p \in A \,|\, \forall_j \neq i,\, d_A(p,K_i) < d_A(p,K_j) \,\}\ . \tag{3.24}$$

Thus, the boundaries of the influence zones constitute the skeletons of influence zones – SKIZs. The boundaries between the various zones of influence give the SKIZ of Y in X, thus:

$$IZ_X(K) = \bigcup IZ_X(K_i)\ ; \tag{3.25}$$

$$SKIZ_X(K) = \frac{X}{IZ_X(K_i)}\ . \tag{3.26}$$

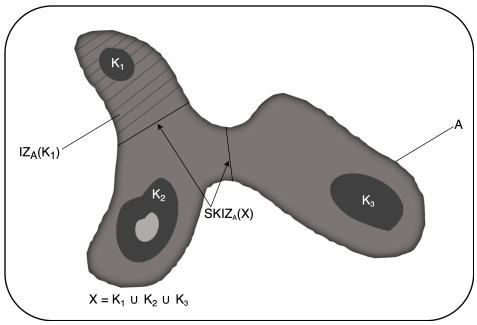

Figure 3.3: Geodesic skeleton and influence zones of three connected components K_1, K_2 and K_3 within a geodesic mask A. The hatched region represents the geodesic influence zone of K_1. Adapted from [46]

3.3.1.3 Definition in terms of flooding simulations

Considering again a given grey tone image as a topographic surface and assuming that holes have been punched in each regional minimum of the surface. Consequently, the water starts entering through the holes and floods the surface. During the flooding, two or more floods coming from different minima may merge; it is desirable to avoid this situation; thus, a dam is built on the points of the surface where the floods would merge. At the end of the process, only the dams emerge. The whole set of dams correspond to the watersheds and provide a partition of the input image into its different catchment basins, each one containing one and only one minimum (Fig. 3.4) [47]. The smallest value taken by the grayscale image f on its domain D_f is denoted by h_{min} and the largest by h_{max}. The catchment basin associated with a minimum M is defined by $CB(M)$. The points of these catchment basin which have an altitude less than or equal to h are defined by $CB_h(M)$:

$$CB_h(M) = \{\, p \in CB_M \,|\, f(p) \leq h \,\} = CB_M \cap T_{t \leq h}(f)\ . \tag{3.27}$$

X_h is defined as the subset of all catchment basins which have a grey scale value less than or equal to h:

$$X_h = \bigcup_i CB_h(M_i)\ . \tag{3.28}$$

Finally, the set of points belonging to the regional minima (Section 3.2.2.3) of elevation h are denoted by $RMIN_h(f)$. Hence, the catchment basins start to be flooded and the first image points that are reached by water are the ones with the lowest grey scale value. These points $T_{h_{min}}$ belong to the $RMIN_h(f)$ at level h_{min}:

$$X_{h_{min}} = T_{h_{min}}(f) = RMIN_{h_{min}}(f)\ . \tag{3.29}$$

While occurring the flooding process, the water either expands within the regions of current CBs or starts to flood CBs whose minima have an altitude equal to h_{min+1}. Thus, there are three possible relations of inclusion (Fig. 3.4) between a connected component Y of $T_{t \leq h_{min+1}}(f)$ and the intersection

between Y and $X_{h_{min}}$:

A. $Y \cap X_{h_{min}} \neq \emptyset$. Consequently, Y is a new regional minimum of f at level h_{min+1} since

$$\forall_p \in Y, \begin{cases} p \notin X_{h_{min}} & \Longrightarrow \quad f(p) \geq h_{min}+1 \; ; \\ p \in Y & \Longrightarrow \quad f(p) \leq h_{min}+1 \; . \end{cases} \tag{3.30}$$

B. $Y \cap X_{h_{min}} \neq \emptyset$ and is connected. In this case, Y exactly corresponds to the pixels belonging to the catchment basin associated with the minimum $Y \cap X_{h_{min}}$ and having a grey level less or equal to $h_{min}+1$:

$$Y = CB_{h_{min}+1}(Y \cap X_{h_{min}}) = IZ_Y(Y \cap X_{h_{min}}) \; . \tag{3.31}$$

C. $Y \cap X_{h_{min}} \neq \emptyset$ and is not connected. Therefore, Y contains more than one minimum of f at level h_{min}. Defining these minima as $Z_1, Z_2, \ldots Z_k$, and let Z_i be one of them. At this point, the best possible approximation for $CB_{h_{min}+1}(Z_i)$ corresponds to the geodesic influence zone of Z_i inside Y:

$$CB_{h_{min}+1}(Z_i) = IZ_Y(Z_i) \; . \tag{3.32}$$

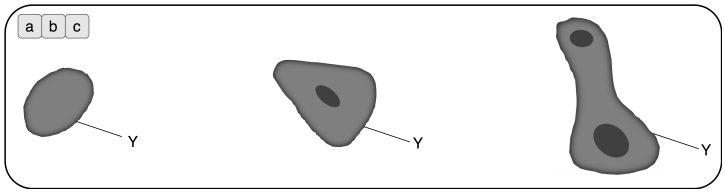

Figure 3.4: Inclusion relations appearing when flooding a grayscale image. Dark grey regions indicate pixels that have already been flooded at level h_{min}, i.e., pixels of $X_{h_{min}}$ ((a),(b) and (c) correspond to A,B and C relations described by Equations 3.30, 3.31, and 3.32, respectively). Adapted from [46]

The regions from B and C relations can be defined in terms of a unique geodesic influence zone, i.e., the IZ of $X_{h_{min}+1}$ within $T_{t \leq h_{min}+1}$. Subsequently, $X_{h_{min}+1}$ can be defined as the union of these geodesic influence zones with the newly discovered regional minima:

$$X_{h_{min}+1} = RMIN_{h_{min}}(f) \cup IZ_{T_{t \leq h_{min}+1}}(f)(X_{h_{min}}) \; . \tag{3.33}$$

This relation holds for all levels h and is exhibited in Figure 3.5. The set of catchment basins of a gray scale image f is equal to the set $X_{h_{max}}$, i.e., once all levels have been flooded:

1.
$$X_{h_{min}} = T_{h_{min}}(f) \; ; \tag{3.34}$$

2.
$$\forall_h \in [\, h_{min},\, h_{max}-1 \,], X_{h+1} = RMIN_{h+1}(f) \cap IZ_{T_{t \leq h_{min}+1}}(f)(X_h) \; . \tag{3.35}$$

Concisely, the result of the Watershed method when applied to the image f corresponds to the set of points from its domain D_f that doesn't belong to any of the CBs. The Watershed method is recognized as one of the most efficient and robust tools in segmentation processes [46, 49]. However, over segmentation is seen as one of its main limitations. Occasionally, when this technique is performed, exaggerated catchment basins are created each of which with an associated local minimum. The over segmentation is a consequence of the excessive local minima, normally induced by noise existent on the image. Moreover, alternative algorithms with an improved local minima detection have been developed [44, 47, 49].

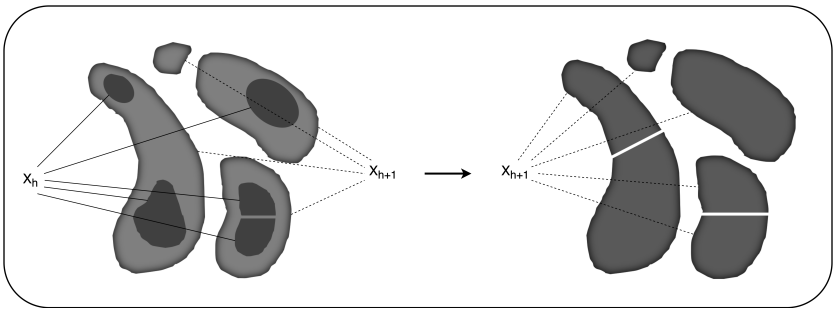

Figure 3.5: Recursion relation between X_h and X_{h+1}.

3.4 Machine Learning and Artificial Intelligence

Machine-learning technology powers many aspects of modern society and is employed in several applications, e.g., object identification in images, speech transcription into text and also in consumer products such as cameras and smartphones. Conventional machine-learning techniques were limited in their ability to process natural data in their raw form and required careful engineering to design a feature extractor that transformed the raw data into a suitable internal representation (e.g. feature vector) for posterior pattern detection/classification. Deep-learning methods are representation--learning methods (procedures that allow a machine to be fed with raw data and automatically discover the representations needed for detection/classification) with multiple levels of representation, obtained by composing simple but non-linear modules that transform the representation at one level into another on a higher level. With the composition of enough such transformations, very complex functions can be learned. For classification tasks, higher layers of representation amplify aspects of the input that are important for discrimination and suppress irrelevant variations. The key aspect of deep learning is that these layers of features are not designed by human engineers: they are learned from data using a general-purpose learning procedure [35, 50].

3.4.1 Supervised Learning

The most common form of machine learning, deep or not, is supervised learning and has inherent stages. First a large data set has to be collected and labelled according to its category: images of different objects, for example. The machine will be fed and trained with the labeled images; during training, the machine will produce an output in a form of a vector of scores, one for each category; after training is expected that the desired category has the highest score. Thereafter, is computed an objective function that measures the error between the output scores and the desired pattern of scores. The machine then modifies its internal adjustable parameters to reduce this error. These adjustable parameters, often called *weights*, define the input-output function of the machine and typically, there are hundreds of millions of these adjustable *weights* in a deep-learning system. To properly adjust the weighted vector, the learning algorithm computes a gradient vector that, for each *weight*, indicates by what amount the error would increase or decrease if the *weight* were increased by a tiny amount. Most practitioners use a procedure called stochastic gradient descent (SGD); consists of showing the input vector for a few examples, computing the outputs and the errors, computing the average gradient for those examples, and adjusting the *weights* accordingly [50].

3.4.2 Convolutional Neural Networks

The most established algorithm among several deep learning models is convolutional neural networks (CNN), a class of artificial neural networks that has been a dominant method in computer vision tasks. CNN is a type of model for processing data that has a grid pattern, such as images, and is a mathematical construct that is typically composed of three types of building blocks: convolution, pooling, and fully connected layers (Fig. 3.7). The first two, perform feature extraction, whereas the third maps the extracted features into final output, such as classification. The convolutional layer plays a key role in CNN, which is composed of a stack of mathematical operations, such as convolution. Convolution (Fig. 3.6) is the linear operation used for feature extraction, where a *kernel* is applied across the input tensor and the *feature map* is obtained. The outputs are then passed through a nonlinear activation function, such as sigmoid or hyperbolic tangent function due to their similarities of a biological neuron behavior. Although, the most common nonlinear activation function used presently is the rectified linear unit (ReLU), which computes the following function:

$$f(x) = \max(0, x) \tag{3.36}$$

which will output the input directly if positive, otherwise, outputs zero. To introduce a translation invariance to small shifts and distortions, and decrease the number of subsequent learnable parameters, the in-plane dimensionality of the *feature maps* is reduced in a downsampling operation by the pooling layers. The most popular operation is *max pooling*, where the maximum value of each *feature map* is extracted, and all the other are discarded. There are no learnable parameters in any of the pooling

layers, whereas filter size, stride and padding are hyperparameters in pooling operations. The output of the final convolution or pooling layer is typically flattened into a vector and connected to one or more fully connected (FC) layers, in which every input is connected to every output by a learnable *weight*. Finally, the extracted features are then mapped in order to perform classification. The final FC layer typically has the same number of outputs as the number of classes.

The step where input data is transformed into output through these layers is called *forward propagation*. On the other hand, the training process (Fig. 3.7) can also be achieved by *backpropagation*, where the output errors are returned to the *net* until the error reaches an acceptable level. When training a network, the *loss function* optimization algorithm also plays an essential role; also referred to as a *cost function*, it measures the compatibility between output predictions of the network. Commonly, used loss functions for multiclass classification is cross entropy, whereas mean squared error is typically applied to regression [51].

Machine learning approaches had been widely used in image processing; [52] designed and tested a bacterial colony counting system with two machine learning procedures: the first one was based on the extraction of morphometric and radiometric features through a Support Vector Machines solution. The second one was based on the design and configuration of a CNN deep learning architecture. In their study, the deep learning approach outperformed the firstly-enunciated one by a large margin, thus they concluded that their CNN technique became a preferable solution for quantification tasks in the context of Full Laboratory Automation systems [7]. In [53] was conducted another work where they presented an evaluation of convolutional neural networks to learn features for mammography mass lesions before feeding them to a classification stage. Experimental results showed that the developed approach is a suitable strategy outperforming the state-of-the-art representation from 79.9% to 86% in terms of area under the *receiver operating characteristic* (ROC) curve. These two examples confirm the increasing use of CNN-based techniques showing their potential particularly on image processing processes.

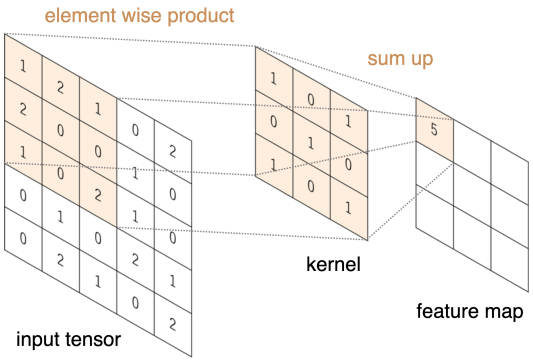

Figure 3.6: Convolution operation with a kernel size of 3×3. The *kernel* is applied across the tensor, and an element-wise product between each element is computed at each location and then summed to obtain the output value in the corresponding position of the feature map. Adapted from [51].

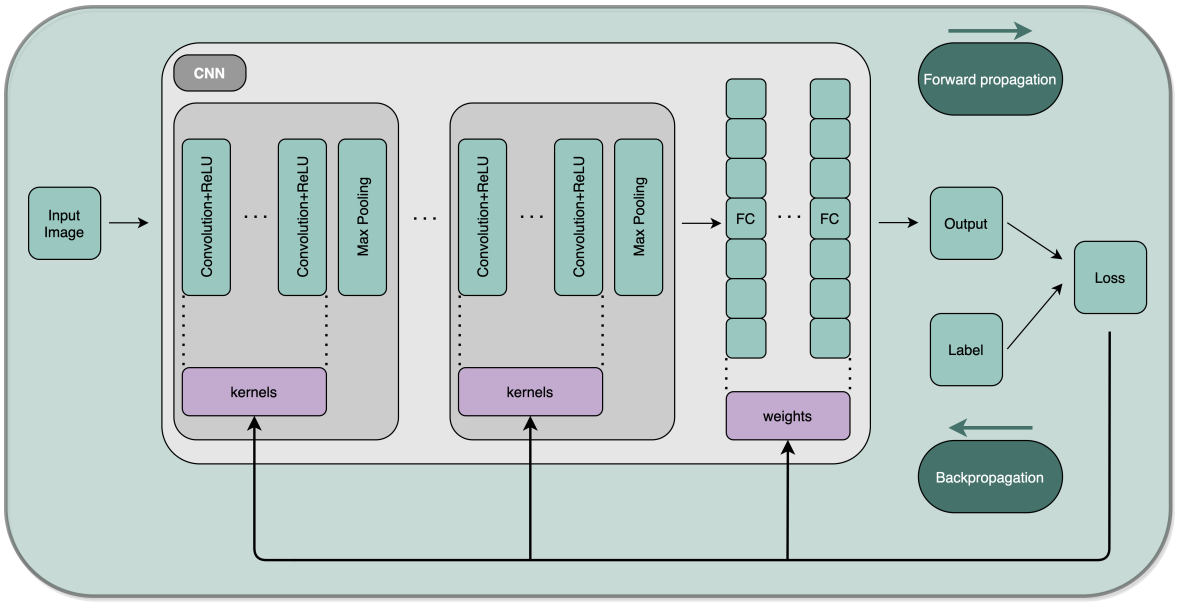

Figure 3.7: Overview of a CNN general architecture and training process. Adapted from [51].

3.4.3 AlexNet

AlexNet is a large, deep CNN that had a remarkable impact in the application of deep learning to machine vision; pretrained on more than a million images from the *ImageNet* database, this network can classify images into 1000 different object categories. Presented during *ImageNet Large-Scale Visual Recognition Challenge's* 2010 edition, AlexNet outperformed the other competing solutions by considerable margins. Its architecture, depicted in Figure 3.8, has by default, eight learned layers – five convolutional and three fully-connected (also known as dense layers), providing the characteristics described in Section 3.4.2. By the time AlexNet was developed, the employment of some novel or unusual architectural features lead to the mentioned achievements. The use of ReLUs enabled the network to train several times faster, improving the performance of the model. A cross-GPU parallelization (two GPUs with half of the neurons each, communicating only in certain layers) was applied to use less memory of each machine, increasing processing capacity. Another component of AlexNet was the overlapping pooling; mentioned in Section 3.4.2, pooling layers summarize the outputs of neighboring groups of neurons. During this operation, pooling units were overlapped, resulting less overfitting of the trained data. The output of the last FC layer was fed to a 1000-way softmax for output normalization and production of a distribution over the 100 class labels [51, 54].

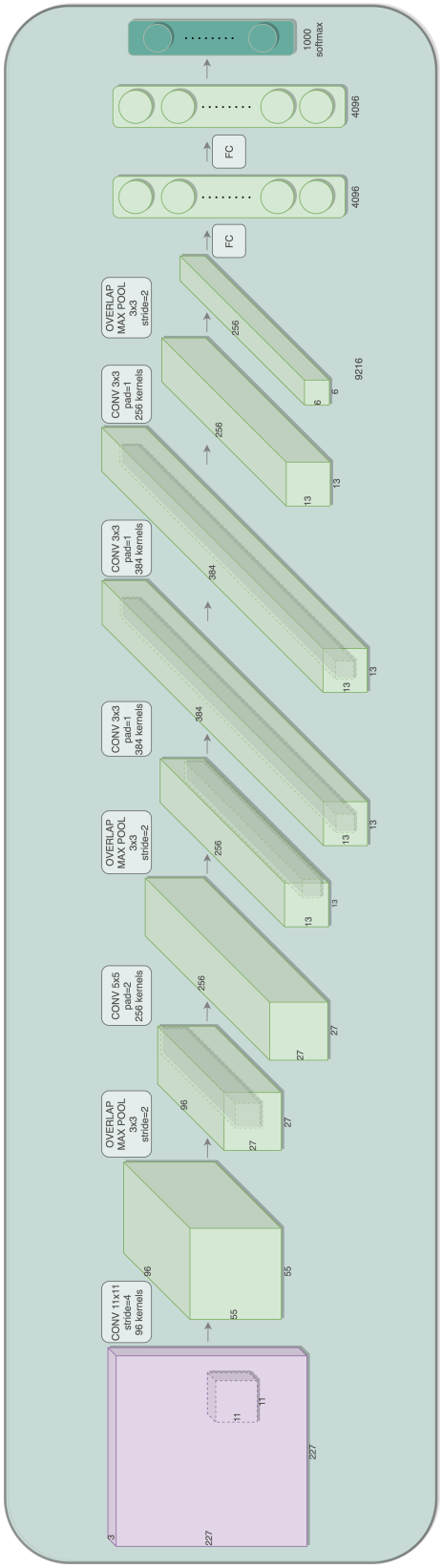

Figure 3.8: AlexNet architecture. Adapted from [54].

CHAPTER 4

Methodology

In this chapter all the developed procedures are described. Primarily, the microbiology methods performed to obtain the image database are detailed. Furthermore, the flowchart of the process (enumeration/distinction) is presented. Ultimately, the overall process is presented in detail with discrimination of each step and sub-step. After an analysis of the database, a set of characteristics were outlined to select the techniques to be implemented; high amount of noise, reduced contrast between fore and background, existing clumps of bacteria, variation of colony size, presence of high intensity areas and inherent plate marks were some of the aspects taken into account. Thus, there was a special concern to develop a set of procedures capable of overcoming the emerged and enunciated adversities, achieving the best results possible. Moreover, there was a concern in building a versatile algorithm, i.e. applicable to images with different properties or acquired through distinct laboratory procedures.

4.1 Bacterial cultures

4.1.1 Origin

For this study, and in particular for the image database conception, three bacterial species were cultivated, *Escherichia coli*, *Pseudomonas aeruginosa* and *Staphylococcus aureus*. The three aerobic bacteria were provenient from the internal collection of CINATE (Center for Innovation and Technological Support within ESB) and were cultivated aerobically at 37°C.

4.1.2 *Escherichia coli*

Escherichia coli is a Gram-negative, rod-shaped bacteria and a member of the family *Enterobacteriaceae* and the *Gammaproteobacteria* class, is the most prevalent commensal inhabitant of the

gastrointestinal tract of humans and warm-blooded animals, as well as one of the most important pathogens. As a commensal, it lives in a mutually beneficial association with the host, and rarely causes disease. However, if found present outside its habitual site it can be responsible for a broad spectrum of diseases. The peculiar characteristics of *E. coli*, such as ease of handling, availability of the complete genome sequence, and its ability to grow under both aerobic and anaerobic conditions, makes it an important host organism in biotechnology. It is likewise used in a wide variety of applications both in the industrial and medical area [55]. Related to its colonial morphology, when cultivated in Brain Hearth Broth (BHI) and Trypticase Soy Agar (TSA), *E. coli* appears gray, mucoid, flat or convex and not swarming [56].

4.1.3 *Pseudomonas aeruginosa*

Pseudomonas aeruginosa is a Gram-negative, rod-shaped bacterium from the *Pseudomonadaceae* family and the *Gammaproteobacteria* class. It is an opportunistic pathogenic bacterium responsible for both acute and chronic infections. Beyond its natural resistance to many drugs, its ability to form biofilm, a complex biological system, renders ineffective the clearance by immune defense systems and antibiotherapy [57]. Its colonies appear flat, gray-green, rough, may have spreading margins, metallic sheen and may be extremely mucoid [56].

4.1.4 *Staphylococcus aureus*

Staphylococcus aureus is a Gram-positive bacteria, from the *Staphylococcaceae* family and the *Bacilli* class, characterized by individual cocci, which divide in more than one plane to form grape-like clusters. It is a non-spore forming, facultative anaerobe that grows either by aerobic respiration or by fermentation and can frequently be found in the upper respiratory tract and on the skin. It is a major pathogen of increasing importance due (likewise *P. aeruginosa*) to the rise in antibiotic resistance [58]. Additionally, it has been identified as the causative agent in many food poisoning outbreaks and is probably responsible for even more cases in individuals and family groups than the records show. Nonetheless, is highly vulnerable to destruction by heat treatment and nearly all sanitizing agents [59]. Regarding the morphology of *S. aureus*, according to the literature, its colonies are large, convex, white-yellow, creamy and opaque [56]. Table 4.1 exhibits an array of some biochemical characteristics of the above-mentioned bacteria.

Table 4.1: Some biochemical characteristics from the three bacteria. Adapted from [56].

	Gram stain	Motility	Coagulase	Oxidase	Glucose	Sucrose	Lactose	Maltose	Fructose
E.coli	−	+	−	−	A	A	−	−	−
P.aeruginosa	−	+	−	−	A	A/G	A/G	−	A
S.aureus	+	−	+	−	A	A/G	A/G	A	A

\+ positive test;
− negative test;
A acid production;
G gas production.

4.2 Culture media

Two general-purpose media were used to grow the 3 bacterial species, Brain-Hearth Broth™ and Trypto-Casein Soy Agar™ both from BIOKAR Diagnostics©, Allonne, France.

Brain-Hearth Broth™ is a buffered nutrient medium used for the culture of a wide variety of aerobic and anaerobic microorganisms. Regarding the typical composition, for 1 liter of media is 17.5 g of pork brain-heart infusion, 10.0 g of pancreatic digest of gelatin, 5.0 g of sodium chloride, 2.5 g of disodium phosphate and 2.0 g of glucose. The pH of the ready-to-use media at 25°C is 7.4 ± 0.2. The typical composition of the broth responds to the formulation described in the Directives NF EN ISO 6888-1, NF EN ISO 6888-3 & NF EN ISO V08-057-1.

Trypto-Casein Soy Agar™ is a universal nutrient medium also suitable for a wide range of uses. Can be used for the growth and isolation of both aerobic and anaerobic bacteria and to favor the development of the most fastidious microorganisms. Its typical composition, for 1 liter of media is 15.0 g tryptone, 5.0 g papaic digest of soybean meal, 5.0 g sodium chloride and 15.0 g of bacteriological agar. The pH of the ready-to-use media at 25°C is 7.3 ± 0.2. Under the determination TSA (Tryptic Soy Agar), this formula corresponds to the reference medium used for the evaluation of productivity and selectivity criteria in the context of the ISO 11133 standard.

4.3 Bacterial growth and quantification

4.3.1 Media preparation

To obtain a liquid media for the inoculum, Brain-Hearth Broth™ was used; 37.0 g of dehydrated medium were dissolved in 1 liter of deionized water. The solution was slowly stirred until complete dissolution. After pipetting 10 mL into test tubes, the media was sterilized in autoclave at 121°C for 17 minutes. Posteriorly, the media tubes were cooled to room temperature.

The solid media to be poured into the petri dishes was prepared with both Brain-Hearth Broth™ and Trypto-Casein Soy Agar™. Since the first media is a broth, 15.0 g of bacteriological agar was added to the 37.0 g of media and dissolved in 1 liter of deionized water. The flask was sterilized in autoclave at 121°C for 17 minutes and after cooling to a temperature of approximately 45°C, 20 mL were poured to each plate. Considering the Trypto-Casein Soy Agar™, 40.0 g of the dehydrated medium were dissolved in 1 liter of deionized water. The previous procedure of sterilizing and pouring was executed again.

Ringer's Solution 1/4 strength was used to prepare serial dilutions; this isotonic solution prevents osmotic shock from occurring when bacteria are removed from their usual environment. The typical composition for 1 liter of solution is 2.250 g sodium chloride, 0.105 g potassium chloride, 0.120 g calcium chloride and 0.050 g sodium hydrogenocarbonate. The pH at 25°C is 7.0 ± 0.2. During its preparation, one tablet was placed in 500 mL of demineralized water and slowly stirred until complete

dilution. Nine milliliters of the solution was then dispensed into test tubes and submitted to the previously-employed sterilizing process.

4.3.2 Inoculum preparation

Frozen cultures of the 3 bacterial species cryopreserved in glass-free mini cryovials at -80°C, were thawed via gentle agitation in a water bath that was set to the normal growth temperature of each bacterial species. The thawing was fast, verified by the melting of all the ice crystals. With prior decontamination of the outer surface using 70% ethanol, each vial was removed from the bath. The entire content of each vial was transferred to sterilized test tubes containing the growth media. As recommended on the product sheets, the 3 cultures were incubated overnight at 37°C.

A quadrant streaking technique was performed to produce isolated/purified colonies. Working at the Bunsen burner and using an inoculation loop, the inoculum is diluted by streaking it across the surface of an agar plate, previously prepared. A small amount of inoculum was collected from each tube with the loop and after streaking each quadrant the loop was flamed. The streaked plate was incubated overnight under 37°C.

With evidence of isolated and pure colonies and using the inoculation loop a single colony was collected and transferred to a sterilized test tube containing 10 mL of fresh media. The new pre-inoculum was incubated overnight under 37°C.

Subsequently, 100 μL were transferred from the preceding solution to a 10 mL test tube containing fresh media – the final inoculum was achieved (Fig. 4.1).

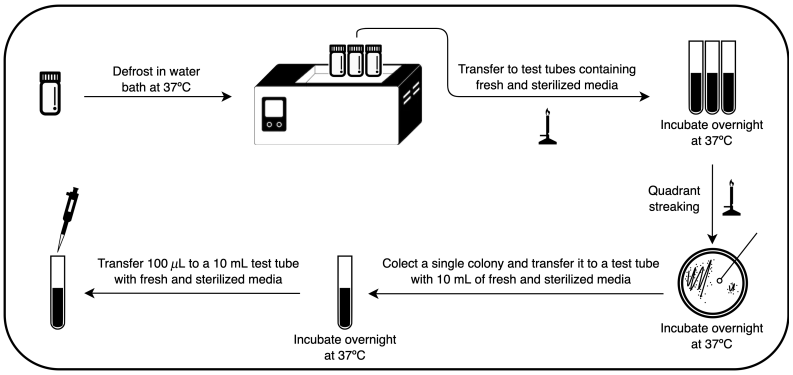

Figure 4.1: Inoculum preparation.

4.3.3 Serial dilutions

After mixing the sample in a vortex, 1 mL of the inoculum was added to a sterilized eppendorf and a centrifugation step was performed. The solutions were centrifuged twice for 10 minutes at 5,000 g, each time resuspended in 1 mL of a Ringer solution previously prepared.

The content of the 3 microorganism solutions was then transferred to sterilized test tubes containing 9 mL of Ringer and the serial dilutions were executed. Each dilution tube contained only one-tenth the number of microbial cells as the preceding tube. The process is represented in Figure 4.2.

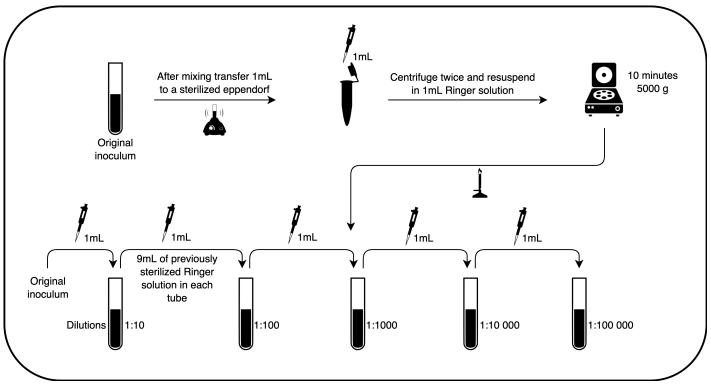

Figure 4.2: Centrifugation and serial dilutions.

4.3.4 Spread Plate and Plate Count Methods

Ultimately, the spread plate method was employed; 100 μL of each dilution were pipetted onto the center of the surface of the sterilized agar plate (prepared ahead). Before spreading the drop, a glass Pasteur pipet was L-shaped, dipped into 96% ethanol, flamed over a Bunsen burner and subsequently, the sample was spread over the surface rotating the Petri-plate underneath at the same time. All cultures used were plated in triplicate, the plates were then incubated overnight under 37°C.

Colony enumeration was performed through the plate count method. The method was performed according to the specified in Chapter 2 and the number of colonies was recorded and posteriorly attributed to each image of the database. The procedure is outlined in Figure 4.3.

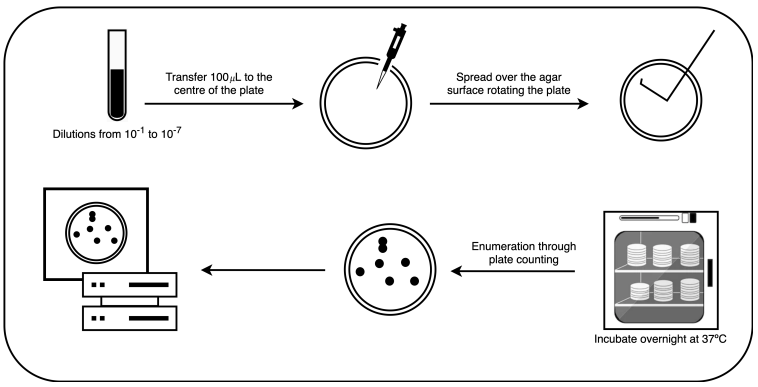

Figure 4.3: Spread plate method.

4.4 Image Database

While developing the image database, the previously described methods (Section 4.3) were performed to obtain accurate plates and with considerable colony-number variability. Subsequently, each manual counting was executed and registered, the plates were then ready for image capture. The image acquisition system used in this study, i.e. a black card box, is shown in Figure 4.4. In order to accentuate the region of interest and provide adequate contrast between the colonies and the background, the 9 cm plate was illuminated from below by two sources of light, aiming for uniformly distributed illumination. A transparent LDPE platform was used to fix the position of the plate. The main purpose of the design of this apparatus is to obtain the images inside the periphery of the plate, including the edge of the periphery. The external light was blocked with the cover of the box, and a PDAF smartphone camera with 12 megapixels (3024×4032) was used to capture the images. Another platform was included to enable the placement of the smartphone always in the same location. With the designed and simple apparatus, good quality images were obtained. Finally, the database was cataloged, attributing number, bacterial species and total manual count to each image, e.g. *CEMTimages_0278_EC_C76*, where *0278*, *EC* and *C76* mean the image number, bacterial species and total count, respectively. The built dataset consists in about 1150 labeled images containing approximately the same amount of each bacterial species.

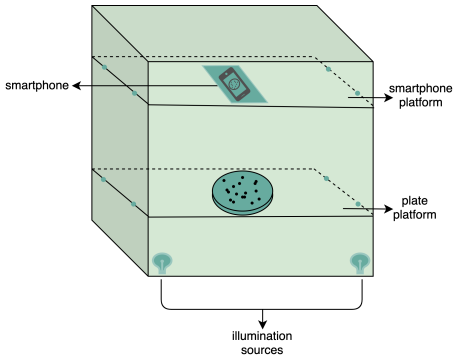

Figure 4.4: Scheme of the handled black box to image acquisition.

4.5 Enumeration process

4.5.1 Overview

From the developed database, data is firstly loaded in MATLAB®; the algorithm performs three major steps: preprocessing, processing and enumeration. Before the preprocessing begins, the user is asked to input a parameter, i.e. the minimum size of a colony. This action is achieved by *imellipse*, an interactive placement of an ellipse around the minimum-sized colony of the plate. Worth to

acknowledge that during the overall process, this is the only occasion the user is asked to input information. Therefore, the computed result is compared with the real labels from each image and consequently the accuracy is achieved. The process is outlined in Figure 4.5.

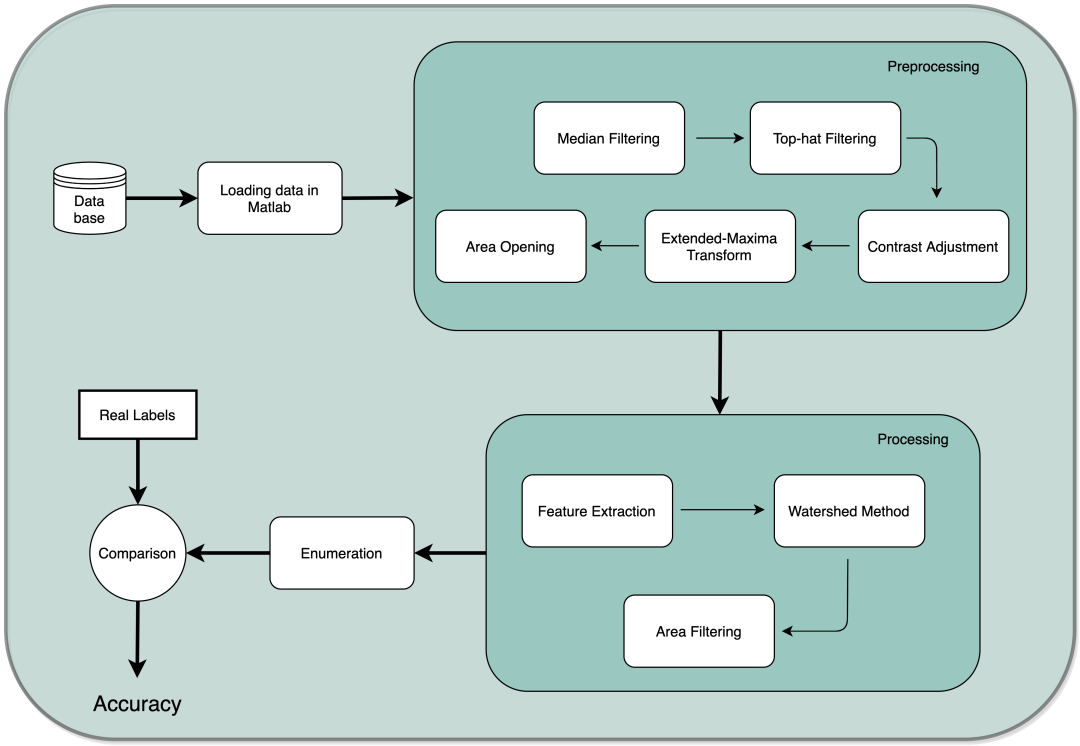

Figure 4.5: Flowchart of the enumeration process.

4.5.2 Preprocessing

Depending on the features of the images under analysis and considered fundamental, preprocessing techniques have extreme relevance in image processing or in any type of signal. Hence, the first stage of the algorithm has the aim to produce the most-satisfactory-possible and noise-free images to further segmentation on the following stage. A summary of the preprocessing stage is presented in Figure 4.11 on page 45.

4.5.2.1 Median Filtering

According to the description addressed in Chapter 3, this technique is widely applied in image processing algorithms, which has useful features regarding the images under analysis, the aim was to reduce the noise without a contrast loss; a 9×9 median filter was adopted, the result is shown in Figure 4.6.

Figure 4.6: Median-filtered image.

4.5.2.2 Top-hat Filtering

To correct possible uneven illumination, which leads to uneven contrast, a top-hat transform with a 200-pixel radius and disk-shaped single structuring element was performed. This morphological filter computes the opening of the image and then subtracts the result from the original (median-filtered image). Figure 4.7 illustrates the result of this step.

Figure 4.7: Tophat transform with a disk structuring element.

4.5.2.3 Contrast Adjustment

On this step (Fig. 4.8) the image was normalized according to Equation 4.1; $p_{adjusted}$ is denoted as the replaced pixel value, p the current pixel value, p_{min} the minimum pixel value, NC the normalization

coefficient and MI the maximum intensity value of the image.

$$\sum_{p_n} p_{adjusted} = \frac{p - p_{min}}{NC} \times MI \tag{4.1}$$

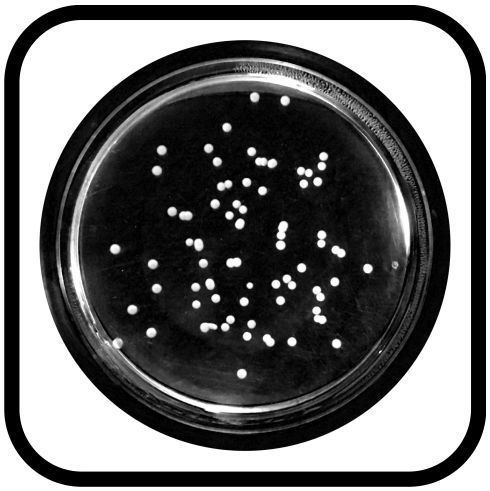

Figure 4.8: Contrast adjustment.

4.5.2.4 Extended-Maximum Transform

Another normalization process occurred; the extended-maxima transform was applied, where the intensities of points inside the foreground regions were changed to show the distance to the closest boundary from each point. First the regional maxima were found; objectively, 80 pixel-region maxima

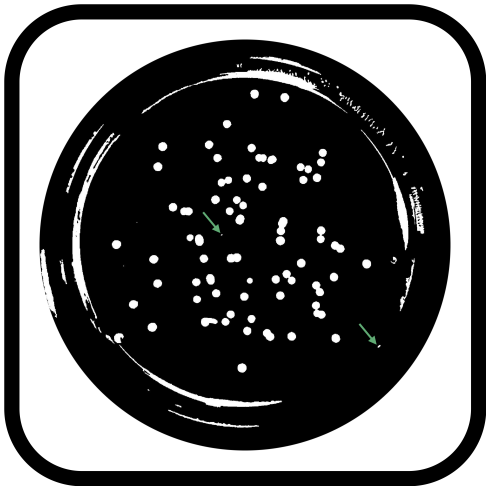

Figure 4.9: Extended-Maximum Transform.

were computed and with 8-connected pixels, i.e. the neighborhood of a pixel are the adjacent pixels in the horizontal, vertical or diagonal direction; subsequently the transformation is performed. The outcome is illustrated in Figure 4.9.

4.5.2.5 Area Opening

The intent of this stage was the removal of small objects from the image (objects marked in Fig. 4.9 with green arrows). All connected components with fewer than 250 pixels were removed. The result is presented in Figure 4.10.

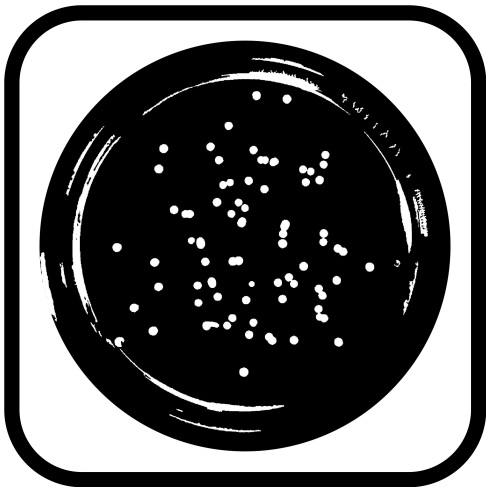

Figure 4.10: Elimination of small objects with less than 250 pixels by performing an area opening operation.

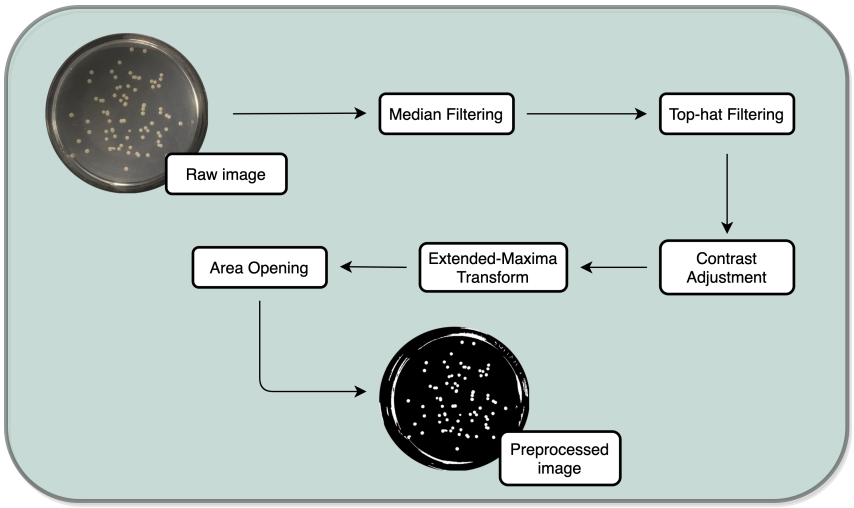

Figure 4.11: Summarized procedures of the preprocessing stage.

4.5.3 Processing

The second main step of the process – processing (summarized in Fig. 4.20 on page 51) – is subdivided in two stages; first the detection of round-shaped objects and posteriorly, the segmentation of the detected round-shaped objects. The objective at this stage is to accomplish isolated colonies to perform an efficient enumeration process.

4.5.3.1 Round-shaped objects detection

The objective of this operation is to select potential colonies. Foremost, from all the detected objects 3 features are extracted: *area*, *perimeter* and *circularity*. From the areas and perimeters, a metric of the "roundness" of the objects is computed, and those objects with a value of 1 are indicative of perfect circles. Since several colonies are not a perfect circle, not only the objects with a metric of 1 are selected but those within an interval, i.e. 0.48 to 1.6. The third extracted feature, circularity, is also a metric of "roundness" and improves the detection procedure. The resulting image is illustrated in Figure 4.12.

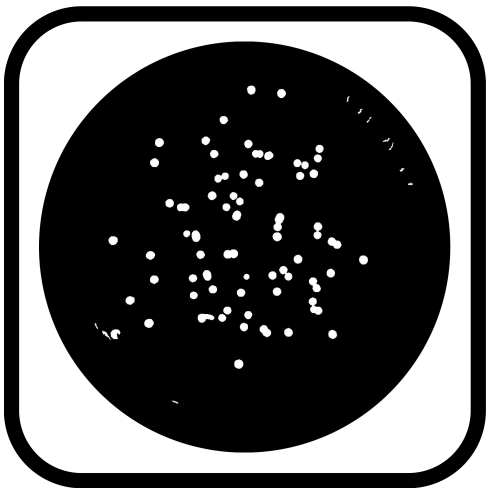

Figure 4.12: Detected round objects.

4.5.3.2 Watershed Method

This phase is important as it transforms the previous image into one where the objects are catchment basins – watersheds, to posteriorly be segmented. The watershed transform is only performed at this stage to avoid over-segmentation issues. This process is subdivided in 5 sub-steps: distance transform, watershed ridges, extended-minima transform, minima imposition and finally the watershed itself.

Distance Transform At this step the distance transform is computed, i.e. the distance from every pixel to the nearest non-zero-valued pixel. However, to turn bright areas into catchment basins and to assign one catchment basin to each object, the distance transform has to be negated (Fig. 4.13).

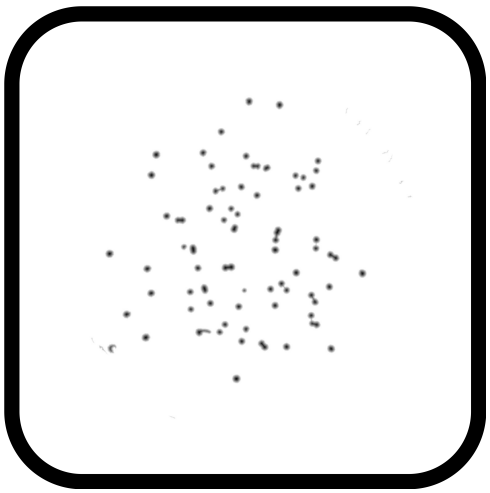

Figure 4.13: Negative of the new distance transform.

Watershed ridges Upon performing the following operation is intended to segment the colonies using the watershed ridges and these values correspond, in fact, to zero; thus, if zero is assigned to those values they become background pixels and subsequently split the colonies. The effects that the aforementioned operation produces are displayed in Figure 4.14.

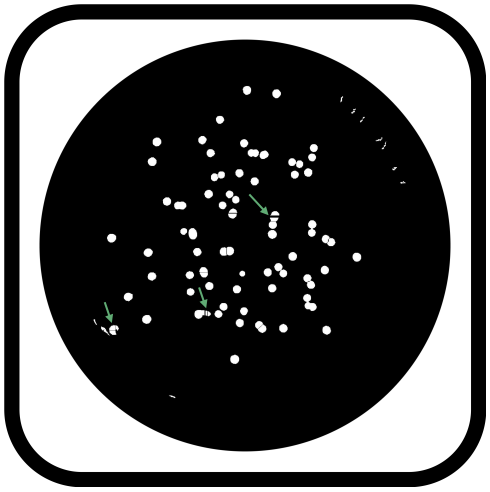

Figure 4.14: Segmentation through watershed ridges; green arrows indicate the effects of this operation.

Extended-Minima Transform Verifiable in the previous figure, the watershed function tends to perform over-segmentations (every local minimum becomes a catchment basin); thus, it is necessary to filter meaningless local minima. Small dots (almost imperceptible) are assigned to each colony and the outcome is shown in Figure 4.15.

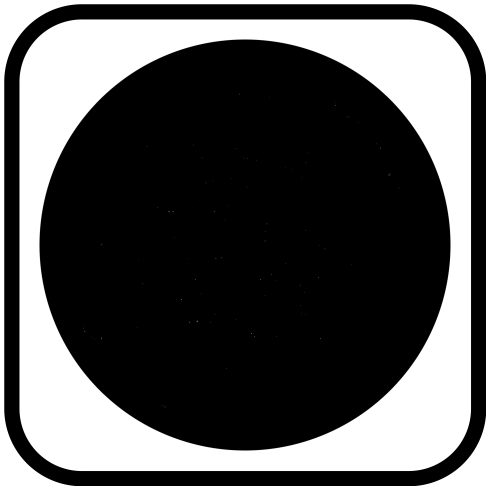

Figure 4.15: Extended-Minimum Transform, assigning small dots to each "true" minima.

Minima imposition The minima imposition technique is related with filtering the image minima. A set of markers is required to identify relevant objects. According to Equation 4.2, the marker image f_m can be defined for each pixel p.

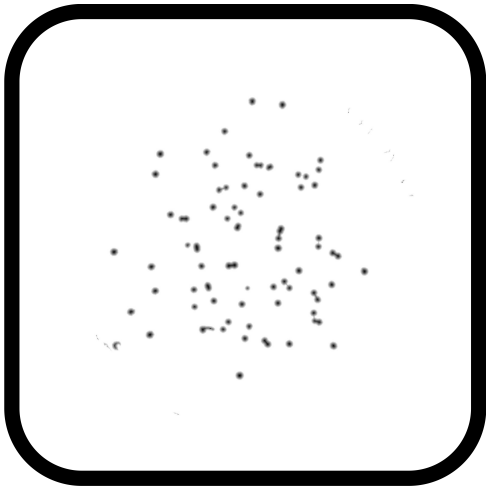

Figure 4.16: Minima imposition.

$$f_m(p) = \begin{cases} 0, & \textit{if p belongs to a marker}\,; \\ t_{max,} & \textit{otherwise}\,. \end{cases} \tag{4.2}$$

The imposition of the minima of the input image is then performed in two steps; first, the pointwise minimum between the input image and the marker image is computed: $f \wedge f_m$. Through the latest, minima are created at locations corresponding to the markers. Moreover, two distinct minima to impose may fall within a minimum of f at level 0, therefore is necessary to consider $(f+1) \wedge f_m$ rather than $f \wedge f_m$. The second step consists in a morphological reconstruction by erosion of $((f+1) \wedge f_m)$ from the marker image f_m:

$$R^{\varepsilon}_{(f+1)\wedge f_m}(f_m)\,; \tag{4.3}$$

the extended transform is then changed in a way that no minima occur in the previously filtered locations. The output of this step is displayed in Figure 4.16.

Watershed Transform Finally, the watershed transform is performed using the watershed function and an image with the segmented colonies is exhibited (Fig. 4.17).

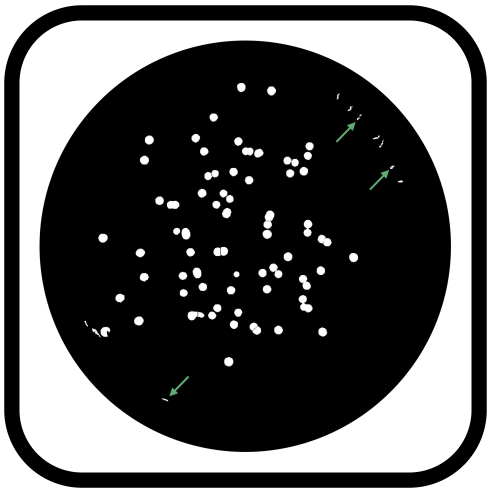

Figure 4.17: Segmented colonies by watershed transform.

Area Filtering At this stage it is necessary to remove artifacts and outliers (pointed in Fig. 4.17 by green arrows) present in the images. All the connected components outside of a specified range are extracted, returning an image containing only those objects that meet the criteria, depicted in Figure 4.18.

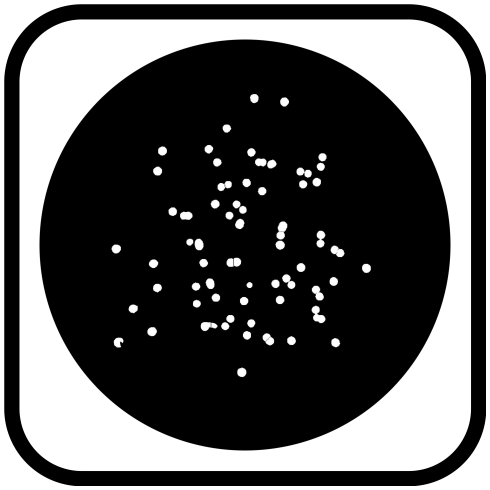

Figure 4.18: Area filtered image.

4.5.4 Enumeration

At this moment the colonies are quantified; the enumeration is performed and displayed on the original image, exhibited in Figure 4.19.

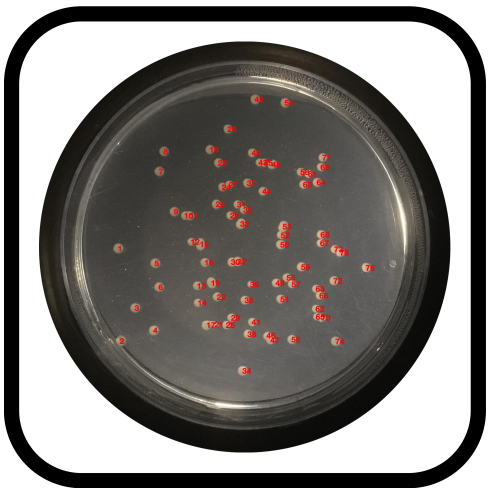

Figure 4.19: Enumerated colonies on the original image.

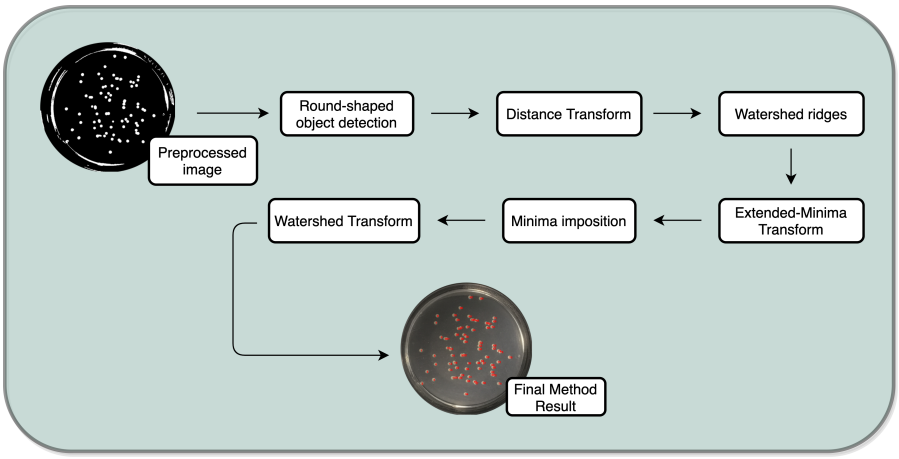

Figure 4.20: Summarized procedures of the processing and enumeration stages.

4.5.5 Classification measurements

After the enumeration stage, a comparison is made with the real label of each image; from the latter comparison is possible to compute the accuracy measures of the enumeration, i.e. precision, recall and F-measure, and consequently access the performance of the overall process.

4.6 Differentiation/Classification process

4.6.1 Overview

The purpose of this process (outlined in Fig. 4.21) is to accurately distinguish the three bacterial groups through the implementation of a CNN using the Deep Learning Toolbox of MATLAB®. After prior separation of the image database into the three above-mentioned groups the images were delivered to the system. Primarily, the images were decimated from their original size format, i.e. converted from 3024×4032 to 227×227. The images were then presented to the AlexNet entries. The classification was performed through cross-validation (leave one out). Ultimately, the accuracy of the classification step is achieved.

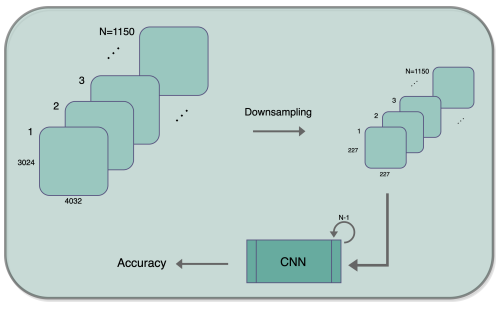

Figure 4.21: Flowchart of the classification process.

CHAPTER 5

Results and Discussion

5.1 General Procedure

The entire method has been described in detail in Sections 4.5 and 4.6 where it is possible to access both processes of enumeration and classification. All particular features were also specified on

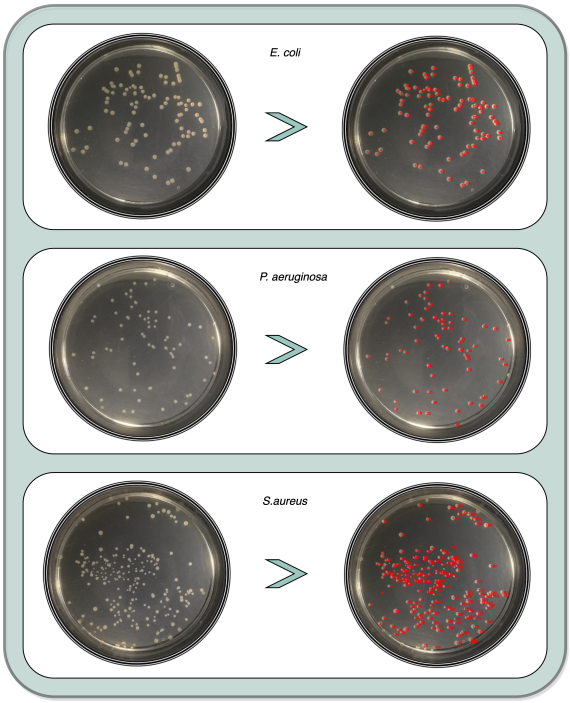

Figure 5.1: Enumeration process exemplified by three inputs (left) and respective outputs (right), one from each bacterial strain.

the above-mentioned sections.To evaluate the efficiency of developed processes, both were tested in all the 1150 images of the database; Figure 5.1 (exhibited on the preceding page) shows three examples (one of each bacteria species) for comparing the input images with the corresponding enumerated-output image.

5.2 Accuracy measurements

5.2.1 Enumeration process

The counting results obtained manually were taken as the real labels, with *true* (colonies) and *false* (non-colonies) cases. The enumeration results obtained by the automated system were the outputs of colony identification, with positive and negative cases, identified as colonies and non-colonies,

Table 5.1: Table of confusion summarizing colonies counted manually and automatically.

		Manual counting	
		True	False
Automated counting	Positive	True Positive (correct result)	False Positive (unexpected result)
	Negative	True Negative (missing result)	False Negative (correct abssence)

respectively. The four possible situations are shown in Table 5.1, where true positives (TP) represents the number of actual colonies identified as colonies; false positives (FP) represents the number of non-colonies incorrectly identified as colonies; false negatives (FN) expresses the number of colonies incorrectly identified as non-colonies; and true negatives (TN) represents the number of non-colonies identified as non-colonies. The precision, also known as positive predictive value, and recall, also known as sensitivity (denoted in [60]) are defined as follows:

$$Precision = \frac{Number\ of\ colonies\ retrieved}{Total\ number\ of\ components\ retrieved} = \frac{TP}{TP+FP}\ ; \tag{5.1}$$

$$Recall = \frac{Number\ of\ colonies\ retrieved}{Total\ number\ of\ existing\ colonies} = \frac{TP}{TP+FN}\ . \tag{5.2}$$

The precision, a measure of exactness was managed by the comparison between the manual counts, i.e. real labels, and the algorithm outputs, and subsequently, Equation 5.1 was applied followed by the average, obtaining the precision value. The same process was adopted to compute the averaged recall value (a measure of completeness), though, using Equation 5.2. An evaluation that combines

precision and recall, F-measure, defined in [60], is denoted as follows:

$$F\text{-}measure = 2 \cdot \frac{precision \cdot recall}{precision + recall} . \tag{5.3}$$

At first, the image database was entirely evaluated and information was gathered about each image in the collected database, specifically, manual counts, algorithm counts, false positives, false negatives and the statistical results; precision, recall and F-measure. From the information aforementioned, three tables were conceived in order to enable a more detailed and comprehensive evaluation of the enumeration process. Table 5.2 exhibits the precision results subdivided in 50-colony-spaced intervals, from [0-50] to "more than 300". Concerning this last interval, worth to mention why it was selected; as mentioned on Section 2.1.2.1, the upper-limit while referring to common acceptance for countable colonies on a plate ranges from 250 to 300, thus plates with more than 300 colonies were simply labeled as "more than 300". Consequently, the precision on that group was computed by verifying if the given plate has in fact more than 300 colonies, if true, the attributed precision was 100%, i.e. if the algorithm performs an enumeration of 326 colonies on an "more than 300" plate (real label) is considered 100% precise, even if the plate itself contain more than 326 colonies (due to the mentioned reasons recall and consequently F-measure were not computed for this group). Table 5.3, expresses similar information as the previous one, although the data is scattered in bigger classes i.e. from [0-100] to [201-300]. On Table 5.4, *E. coli*, *P. aeruginosa* and *S. aureus* images were separately analyzed in order to evaluate the precision of the process concerning each species. To access the overall precision, the respective data was divided into two major classes: [0-300] and more than 300. The above-mentioned tables are exhibited below and on the next page.

Table 5.2: Precision, Recall and F-measure results discriminated into seven groups.

Interval	Precision	Recall	F-measure
0-50	90%	91%	0.91
51-100	92%	93%	0.93
101-150	87%	89%	0.88
151-200	88%	90%	0.89
201-250	84%	87%	0.85
251-300	81%	86%	0.82
More than 300	94%	–	–
Others	74%	80%	0.77

Table 5.3: Precision, Recall and F-measure results discriminated into three groups.

Group	Precision	Recall	F-measure
0-100	91%	92%	0.92
101-200	88%	90%	0.89
201-300	82%	86%	0.84
More than 300	94%	–	–

Table 5.4: Precision, Recall and F-measure results sorted by bacterial species.

Bacteria	Precision		Recall	F-measure
	0-300	More than 300	0-300	0-300
E. coli	95%	96%	95%	0.95
P. aeruginosa	90%	93%	91%	0.90
S. aureus	84%	94%	86%	0.85

From the analysis of Tables 5.2 and 5.3, satisfying results are exhibited, roughly between 80% and 92%. Accuracy measures tend to decrease with the increasing of the colony number, as expected. This latter circumstance is more perceptible in the "Others" class, a group formed by specifically catalogued and overcrowded plates. Nevertheless, in terms of relevance, for a technician or a researcher it is often enough to know that the plate is above 300 colonies. Regarding the mentioned acknowledgement, the method demonstrates efficiency with 93% precision on the "more than 300" group. From Table 5.4, accuracy results of *E. coli* should be highlighted, evidencing values of 95%. In addition, in Figure 5.2 (presented on the facing page) is shown the overall correlation (excluding "more than 300" class) between the automated and the manual counts, indicating a correlation coefficient (R) of 0.9792 and thus, highly correlated data.

While examining the effects of the parameters handled on Equations 5.1 and 5.2, they obviously affect statistical results, where a large number of false positives and false negatives will lower precision and recall, respectively. Expressly, in this work, the false positives resulted from: condensation droplets on the plates' walls, clumps derived from less effective spreading, agar defects in the Petri-plates, a small round-shaped mark inherent on each plate, and residual noise resulting from incomplete elimination during the processing. The causes for the false negative cases are due to: colonies located exactly on the rim of the plate which are eliminated during processing, and concatenated colonies are sometimes wrongly excluded because of their non-circularity or exaggerated area. Additionally, during

the only input required to the user, i.e. selection of the minimum colony size, (at the beginning of the computation) if the colony is missed or wrongly selected, inconsistencies could occur in specific situations. Summarily, the enumeration system evidences consistent accuracy which can be further reinforced by overcoming the above-mentioned limitations.

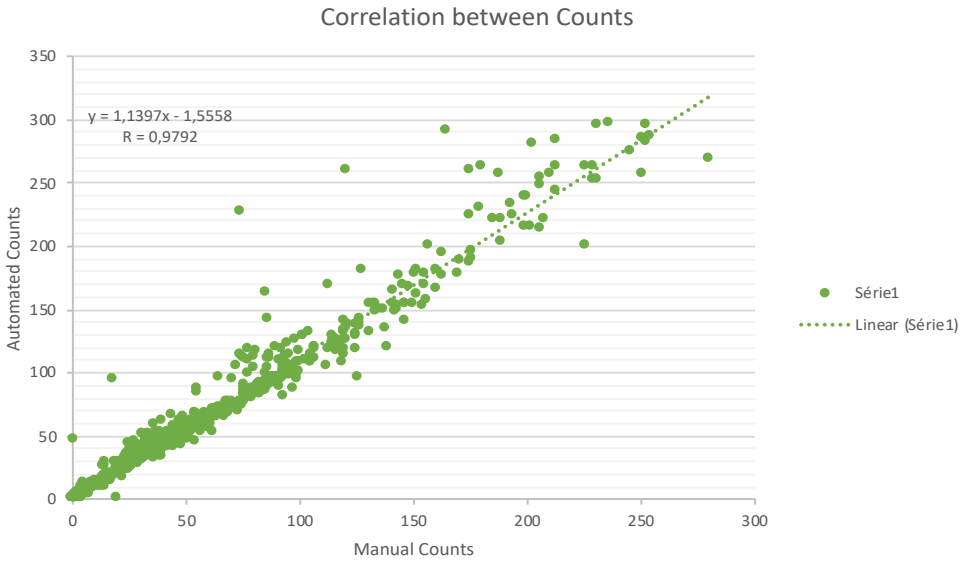

Figure 5.2: Graphical correlation between automated and manual counts.

5.2.2 Classification process

The accuracy of the deep learning-based classification system was accomplished through the training process exhibited in Figure 5.3. It is possible to access the trajectory of the training progress onto two metrics, the accuracy function and additionally, the loss function. The outputs are displayed on the next page (Fig. 5.3 and Table 5.5).

While performing the training process, the learning phase has been performed applying the AlexNet, with its default properties, addressed in Section 3.4.3. The options for training the network were the following: root mean squared propagation (rmsprop) as the training algorithm, a constant learning rate of 0.00001, 50 epochs and 700 iterations. From Figure 5.3, it is verifiable that both accuracy and loss functions express good convergence. The accuracy of the test set was 90.31%, i.e. among the 3 bacterial groups under analysis, the system demonstrated 90.31% accuracy to effectively distinguish those groups.

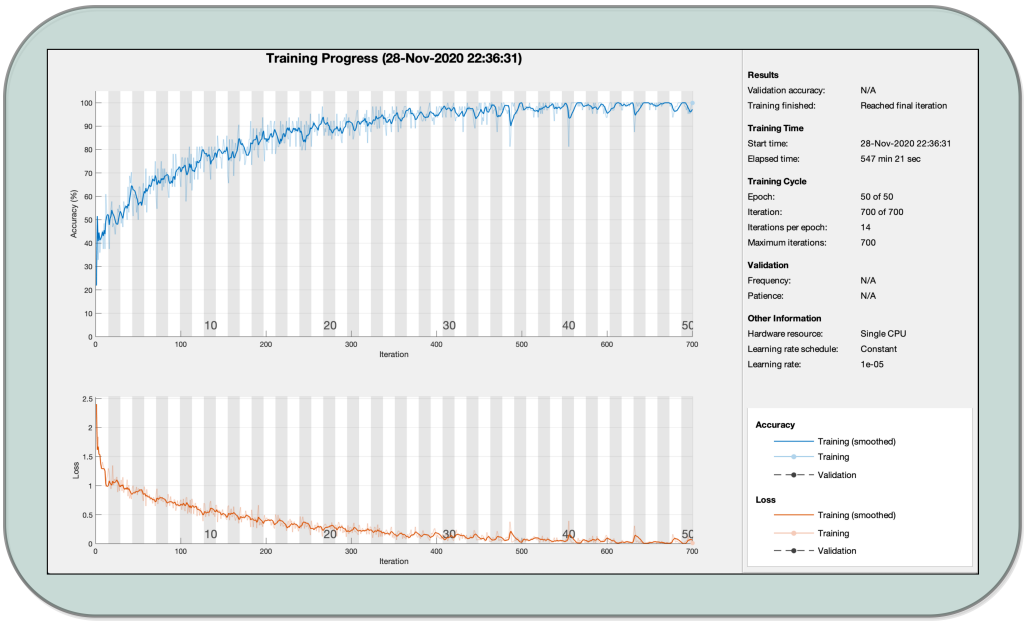

Figure 5.3: Resultant training curves.

Table 5.5: Output parameters of the training process.

Epoch	Iteration	Time Elapsed (hh:mm:ss)	Mini-batch Accuracy	Mini-batch Loss
1	1	0:00:45	21.88%	2.4041
4	50	0:38:54	50.00%	0.9506
8	100	1:17:46	64.06%	0.7557
11	150	1:56:39	84.38%	0.4741
15	200	2:35:27	82.81%	0.4372
18	250	3:14:18	90.62%	0.2591
22	300	3:53:21	90.62%	0.2671
25	350	4:32:19	96.88%	0.0918
29	400	5:11:15	98.44%	0.0986
33	450	5:50:24	100.00%	0.0629
36	500	6:29:30	96.88%	0.0361
40	550	7:08:40	100.00%	0.0336
43	600	7:48:21	93.75%	0.1180
47	650	8:27:46	96.88%	0.0378
50	700	9:07:21	100.00%	0.0119

5.3 Exercise for the Response time workload

The speed of the developed algorithm hinges on the processing capacity of the computer used and on colony size, however the below-presented estimation was obtained based on average values between minor and major computation time intervals. Speed tests were executed on an Intel® i5

CPU running at 2.4 GHz. The execution times of the overall process ranges from 36 seconds to 44 seconds in 30 and 300 colonies, respectively. Table 5.6 reveals the approximated execution times of both manual and algorithm counts, associated with the number of colonies in the plate; the elected number of colonies ranged from 30 to 300.

Table 5.6: Response times tests of the enumeration algorithm.

# Colonies	t_{manual} (s)	$t_{algorithm}$ (s)
30	20	36
50	27	37
100	58	38
150	83	40
200	109	41
250	136	42
300	162	44

Based on Table 5.6, in terms of time management, an exercise could be made (represented in Fig. 5.4) addressing some implications if adopted an automated enumeration procedure:

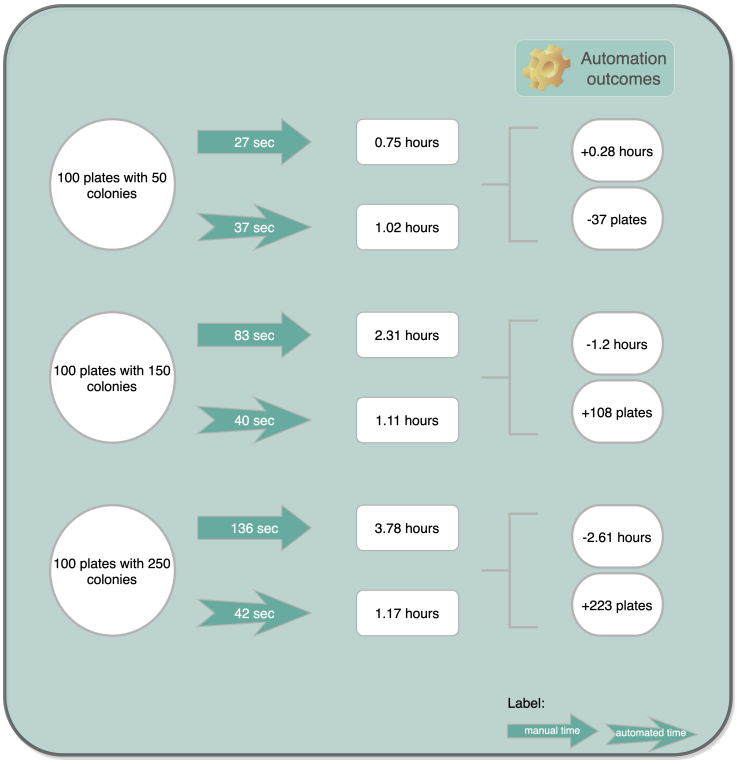

Figure 5.4: Exercise of time management with an automated enumeration process.

CHAPTER 6

Conclusions and Future Work

This work proposed and validated a semi-automated colony counting system and a CNN-based classification system. It was demonstrated to be capable of counting the number of *E. coli*, *P. aeruginosa* and *S. aureus* within acceptable rates of accuracy. For *E. coli*, the mean values of precision, recall and F-measure were 95%, 95% and 0.95, respectively. Respecting the previous order, resultant values for *P. aeruginosa* were 91%, 91% and 0.90, respectively. The outcomes of *S. aureus* were 84%, 86% and 0.85, respectively. Thus, is concludable that *E. coli* is the most-efficiently-detected strain. Respecting the overall and mean values of precision, recall and F-measure, those were 91%, 92% and 0.92; 88%, 90% and 0.89, as well as 82%, 86% and 0.84, categorically split in [0,100], [101,200] and [201,300] intervals. The results of the more than 300 colonies were very satisfactory with a mean precision value of 94%. In addition, *E. coli*, *P. aeruginosa* and *S. aureus* are round in shape; therefore, the proposed counting approach can be applied to any bacterial strain that develops round-shaped colonies. Dry cracks in the agar, poorly performed spreading techniques and illumination inconsistencies might lead to difficulties in the processing of the images and should therefore be avoided during culturing and image acquisition. The proposed counting system is capable of reducing the manpower as well as lowering the time required for counting colonies in half and in one third in some situations, resulting in improved efficiency and productivity of the technician or researcher. However, since during image acquisition, the Petri-plate was illuminated using backlighting, images acquired from plates with non-transparent media might not be easily captured by the employed apparatus. Furthermore, the image processing procedures were developed based on features of colonies with transparent media, and thereby media with diverse colors and opacity might induce unsatisfactory outcomes. The employed Convolutional Neural Net accomplished reliable results manifesting 90.31% of accuracy on the distinction among strains, which suggest robustness, given that all the studied bacterial species are round-shaped and evidence relatively similar visual aspects. Addressing prospect works, certain efforts could be made in order to improve the presented solution; combine both systems

resulting in a robust image processing/analysis tool, provide a more comprehensive counting system with the capability of analyzing a diversified set of microorganisms apart from round-shaped, a graphical user interface (GUI) to promote an enhanced experience to the user and possibly experiment a larger database, empowering the statistical significance. These suggestions might possibly expand the application range of the system and provide an advantageous mechanism to microbiology and biomedicine researchers, contributing to a sustainable laboratory automation.

Bibliography

[1] M. L. Clarke, R. L. Burton, A. N. Hill, M. Litorja, M. H. Nahm, and J. Hwang. "Low-cost, high-throughput, automated counting of bacterial colonies". In: *Cytometry Part A* 77A.8 (2010), pp. 790–797. DOI: 10.1002/cyto.a.20864.

[2] M. Niyazi, I. Niyazi, and C. Belka. "Counting colonies of clonogenic assays by using densitometric software". In: *Radiation Oncology* 2.1 (2007). DOI: 10.1186/1748-717x-2-4.

[3] C. Zhang, W. B. Chen, W. L. Liu, and C. B. Chen. "An Automated Bacterial Colony Counting System". In: *2008 IEEE International Conference on Sensor Networks, Ubiquitous, and Trustworthy Computing (SUTC 2008)*. IEEE, 2008. DOI: 10.1109/sutc.2008.50.

[4] S. D. Brugger, C. Baumberger, M. Jost, W. Jenni, U. Brugger, and K. Mühlemann. "Automated Counting of Bacterial Colony Forming Units on Agar Plates". In: *PLoS ONE* 7.3 (2012). Ed. by S. Bereswill, e33695. DOI: 10.1371/journal.pone.0033695.

[5] Q. Geissmann. "OpenCFU, a New Free and Open-Source Software to Count Cell Colonies and Other Circular Objects". In: *PLoS ONE* 8.2 (2013). Ed. by R. M. Merks, e54072. DOI: 10.1371/journal.pone.0054072.

[6] S. Trattner, H. Greenspan, G. Tepper, and S. Abboud. "Automatic Identification of Bacterial Types Using Statistical Imaging Methods". In: *IEEE Transactions on Medical Imaging* 23.7 (2004), pp. 807–820. DOI: 10.1109/tmi.2004.827481.

[7] A. Ferrari, S. Lombardi, and A. Signoroni. "Bacterial colony counting with Convolutional Neural Networks in Digital Microbiology Imaging". In: *Pattern Recognition* 61 (2017), pp. 629–640. DOI: 10.1016/j.patcog.2016.07.016.

[8] W. M. Ahmed, B. Bayraktar, A. K. Bhunia, E. D. Hirleman, J. P. Robinson, and B. Rajwa. "Classification of Bacterial Contamination Using Image Processing and Distributed Computing". In: *IEEE Journal of Biomedical and Health Informatics* 17.1 (2013), pp. 232–239. DOI: 10.1109/titb.2012.2222654.

[9] W. B. Chen and C. Zhang. "An automated bacterial colony counting and classification system". In: *Information Systems Frontiers* 11.4 (2009), pp. 349–368. DOI: 10.1007/s10796-009-9149-0.

[10] A. Ferrari and A. Signoroni. "Multistage classification for bacterial colonies recognition on solid agar images". In: *2014 IEEE International Conference on Imaging Systems and Techniques (IST) Proceedings*. IEEE, 2014. DOI: 10.1109/ist.2014.6958454.

[11] M. Madigan. *Brock Biology of Microorganisms*. Boston: Pearson, 2015. ISBN: 9780321897398.

[12] G. Tortora. *Microbiology : an Introduction*. Boston: Pearson, 2019. ISBN: 9780134605180.

[13] C. Laplace-Builhé, K. Hahne, W. Hunger, Y. Tirilly, and J. Drocourt. "Application of flow cytometry to rapid microbial analysis in food and drinks industries". In: *Biology of the Cell* 78.1-2 (1993), pp. 123–128. DOI: 10.1016/0248-4900(93)90122-u.

[14] V. Beloti, M. de Aguiar Ferreira Barros, L. A. Nero, J. A. de Souza Pachemshy, E. H. W. de Santana, and B. D. Franco. "Quality of pasteurized milk influences the performance of ready-to-use systems for enumeration of aerobic microorganisms". In: *International Dairy Journal* 12.5 (2002), pp. 413–418. DOI: 10.1016/s0958-6946(02)00021-3.

[15] E. L. Joachimsthal, V. Ivanov, J. H. Tay, and S. T. L. Tay. "Flow cytometry and conventional enumeration of microorganisms in ships' ballast water and marine samples". In: *Marine Pollution Bulletin* 46.3 (2003), pp. 308–313. DOI: 10.1016/s0025-326x(02)00401-0.

[16] L. G. Lehmicke, R. T. Williams, and R. L. Crawford. "14C-most-probable-number method for enumeration of active heterotrophic microorganisms in natural waters." In: *Applied and Environmental Microbiology* 38.4 (1979), pp. 644–649. DOI: 10.1128/aem.38.4.644-649.1979.

[17] S. Galvin, A. Dolan, O. Cahill, S. Daniels, and H. Humphreys. "Microbial monitoring of the hospital environment: why and how?" In: *Journal of Hospital Infection* 82.3 (2012), pp. 143–151. DOI: 10.1016/j.jhin.2012.06.015.

[18] K Maquelin, C Kirschner, L. P Choo-Smith, N van den Braak, H. Endtz, D Naumann, and G. Puppels. "Identification of medically relevant microorganisms by vibrational spectroscopy". In: *Journal of Microbiological Methods* 51.3 (2002), pp. 255–271. DOI: 10.1016/s0167-7012(02)00127-6.

[19] R. Dutton, G. Bitton, and B. Koopman. "Application of a direct microscopic method of the determination of active bacteria in lakes". In: *Water Research* 20.11 (1986), pp. 1461–1464. DOI: 10.1016/0043-1354(86)90147-8.

[20] S. Sutton. "Accuracy on plate counts". In: *Journal of Validation Technology* (2011).

[21] J. E. Gilchrist, J. E. Campbell, C. B. Donnelly, J. T. Peeler, and J. M. Delaney. "Spiral Plate Method for Bacterial Determination". In: *Applied Microbiology* 25.2 (1973), pp. 244–252. DOI: 10.1128/am.25.2.244-252.1973.

[22] M. Fakruddin, K. S. B. Mannan, and S. Andrews. "Viable but Nonculturable Bacteria: Food Safety and Public Health Perspective". In: *ISRN Microbiology* 2013 (2013), pp. 1–6. DOI: 10.1155/2013/703813.

[23] M. Alam, M. Sultana, G. B. Nair, A. K. Siddique, et al. "Viable but nonculturable Vibrio cholerae O1 in biofilms in the aquatic environment and their role in cholera transmission". In: *Proceedings of the National Academy of Sciences* 104.45 (2007), pp. 17801–17806. DOI: 10.1073/pnas.0705599104.

[24] M. Alexander. "Most-Probable-Number Method for Microbial Populations". In: *Agronomy Monographs*. American Society of Agronomy, Soil Science Society of America, 2016, pp. 1467–1472. DOI: 10.2134/agronmonogr9.2.c49.

[25] N. R. Ziegler and H. O. Halvorson. "Application of Statistics to Problems in Bacteriology". In: *Journal of Bacteriology* 29.6 (1935), pp. 609–634. DOI: 10.1128/jb.29.6.609-634.1935.

[26] O. W. W. Reif. "Microfiltration Membranes: Characteristics and Manufacturing". In: *Sterile Filtration*. Springer-Verlag, pp. 73–103. DOI: 10.1007/b104245.

[27] S. Y. Lee, S. S. Chang, J. H. Shin, and D. H. Kang. "Membrane filtration method for enumeration and isolation of *Alicyclobacillus spp.* from apple juice". In: *Letters in Applied Microbiology* 45.5 (2007), pp. 540–546. DOI: 10.1111/j.1472-765x.2007.02229.x.

[28] O Nybroe. "Assessment of metabolic activity of single bacterial cells – new developments in microcolony and dehydrogenase assays". In: *FEMS Microbiology Ecology* 17.2 (1995), pp. 77–83. DOI: 10.1016/0168-6496(95)00013-z.

[29] E. Li and R. M. de Orduña. "A rapid method for the determination of microbial biomass by dry weight using a moisture analyser with an infrared heating source and an analytical balance". In: *Letters in Applied Microbiology* 50.3 (2010), pp. 283–288. DOI: 10.1111/j.1472-765x.2009.02789.x.

[30] K. Kiviharju, K. Salonen, U. Moilanen, and T. Eerikäinen. "Biomass measurement online: the performance of in situ measurements and software sensors". In: *Journal of Industrial Microbiology & Biotechnology* 35.7 (2008), pp. 657–665. DOI: 10.1007/s10295-008-0346-5.

[31] J. Moldenhauer. "Validation of Rapid Microbiological Methods (RMMs)". In: *Sterile Product Development*. Springer New York, 2013, pp. 513–534. DOI: 10.1007/978-1-4614-7978-9_20.

[32] J. W. S. Ronald M. Atlas. *Handbook of Media for Clinical and Public Health Microbiology*. Taylor & Francis Ltd., Oct. 2013. 578 pp. ISBN: 9781466582934.

[33] E. R. Angert. "Alternatives to binary fission in bacteria". In: *Nature Reviews Microbiology* 3.3 (2005), pp. 214–224. DOI: 10.1038/nrmicro1096.

[34] D. Mara and N. Horan. *Handbook of Water and Wastewater Microbiology*. ACADEMIC PR INC, Sept. 2003. 832 pp. ISBN: 0124701000.

[35] R. Gonzalez and R. Woods. *Digital Image Processing*. New York, NY: Pearson, 2018. ISBN: 9780133356724.

[36] W. Burger and M. J. Burge. *Principles of Digital Image Processing*. Springer London, 2009. DOI: 10.1007/978-1-84800-191-6.

[37] C. Solomon. *Fundamentals of Digital Image Processing : a practical approach with examples in Matlab*. Chichester: Wiley-Blackwell, 2011. ISBN: 9780470844724.

[38] R. Staunton. "Hexagonal Sampling in Image Processing". In: *Advances in Imaging and Electron Physics*. Elsevier, 1999, pp. 231–307. DOI: 10.1016/s1076-5670(08)70188-5.

[39] R. Geng and Y. Gong. "High performance active image sensor pixel design with circular structure oxide TFT". In: *Journal of Semiconductors* 40.2 (2019), p. 022402. DOI: 10.1088/1674-4926/40/2/022402.

[40] E. R. Davies. *Computer Vision*. Elsevier LTD, Oxford, Oct. 2017. ISBN: 012809284X.

[41] G. Kaur and P. Sethi. "A Novel Methodology for Automatic Bacterial Colony Counter". In: *International Journal of Computer Applications* 49.15 (2012), pp. 21–26. DOI: 10.5120/7704-1061.

[42] M. A. Koli. "Review of Impulse Noise Reduction Techniques". In: *International Journal Computer Science Engineering* 4.222222 (2012), pp. 184–196.

[43] T. Huang, G. Yang, and G. Tang. "A fast two-dimensional median filtering algorithm". In: *IEEE Transactions on Acoustics, Speech, and Signal Processing* 27.1 (1979), pp. 13–18. DOI: 10.1109/tassp.1979.1163188.

[44] P. Soille. *Morphological Image Analysis*. Springer Berlin Heidelberg, Nov. 2010. 408 pp. ISBN: 3642076963.

[45] R. Gonzalez, R. Woods, and S. Eddins. *Digital Image Processing using MATLAB*. Upper Saddle River, NJ: Pearson/Prentice Hall, 2004. ISBN: 0130085197.

[46] L. Vincent and P. Soille. "Watersheds in digital spaces: an efficient algorithm based on immersion simulations". In: *IEEE Transactions on Pattern Analysis and Machine Intelligence* 13.6 (1991), pp. 583–598. DOI: 10.1109/34.87344.

[47] S. Beucher. "The watershed transformation applied to image segmentation". In: *Scanning Microscopy International*. Vol. suppl. 6. 1992, pp. 299–314.

[48] L. Vincent. "Morphological grayscale reconstruction in image analysis: applications and efficient algorithms". In: *IEEE Transactions on Image Processing* 2.2 (1993), pp. 176–201. DOI: 10.1109/83.217222.

[49] C. Vachier and F. Meyer. "The Viscous Watershed Transform". In: *Journal of Mathematical Imaging and Vision* 22.2-3 (2005), pp. 251–267. DOI: 10.1007/s10851-005-4893-3.

[50] Y. LeCun, Y. Bengio, and G. Hinton. "Deep learning". In: *Nature* 521.7553 (2015), pp. 436–444. DOI: 10.1038/nature14539.

[51] R. Yamashita, M. Nishio, R. K. G. Do, and K. Togashi. "Convolutional neural networks: an overview and application in radiology". In: *Insights into Imaging* 9.4 (2018), pp. 611–629. DOI: 10.1007/s13244-018-0639-9.

[52] A. Ferrari, S. Lombardi, and A. Signoroni. "Bacterial colony counting by Convolutional Neural Networks". In: *2015 37th Annual International Conference of the IEEE Engineering in Medicine and Biology Society (EMBC)*. IEEE, 2015. DOI: 10.1109/embc.2015.7320116.

[53] J. Arevalo, F. A. González, R. Ramos-Pollán, J. L. Oliveira, and M. A. G. Lopez. "Representation learning for mammography mass lesion classification with convolutional neural networks". In: *Computer Methods and Programs in Biomedicine* 127 (2016), pp. 248–257. DOI: 10.1016/j.cmpb.2015.12.014.

[54] A. Krizhevsky, I. Sutskever, and G. E. Hinton. "ImageNet classification with deep convolutional neural networks". In: *Communications of the ACM* 60.6 (2017), pp. 84–90. DOI: 10.1145/3065386.

[55] N. Allocati, M. Masulli, M. Alexeyev, and C. D. Ilio. "*Escherichia coli* in Europe: An Overview". In: *International Journal of Environmental Research and Public Health* 10.12 (2013), pp. 6235–6254. DOI: 10.3390/ijerph10126235.

[56] L. Garcia. *Clinical Microbiology Procedures Handbook*. Washington, DC: ASM Press, 2010. ISBN: 9781555815271.

[57] T. Rasamiravaka, Q. Labtani, P. Duez, and M. E. Jaziri. "The Formation of Biofilms by *Pseudomonas aeruginosa*: A Review of the Natural and Synthetic Compounds Interfering with Control Mechanisms". In: *BioMed Research International* 2015 (2015), pp. 1–17. DOI: 10.1155/2015/759348.

[58] L. Harris, S. Foster, and R. Richards. "An introduction to *Staphylococcus aureus*, and techniques for identifying and quantifying *S. aureus* adhesins in relation to adhesion to biomaterials: review". In: *European Cells and Materials* 4 (2002), pp. 39–60. DOI: 10.22203/ecm.v004a04.

[59] R. W. B. Sandra Tallent Jennifer Hait and G. A. Lancette. *BAM Chapter 12:Staphylococcus aureus*. Available at https://www.fda.gov/food/laboratory-methods-food/bam-chapter-12-staphylococcus-aureus, last accessed in 19 October 2020.

[60] S. V. Stehman. "Selecting and interpreting measures of thematic classification accuracy". In: *Remote Sensing of Environment* 62.1 (1997), pp. 77–89. DOI: 10.1016/s0034-4257(97)00083-7.